# UNCERTAINTY ESTIMATION IN SOUND SCATTERING MEASUREMENTS WITHIN AN ANECHOIC CHAMBER

Master's Thesis in Physics

by

ISABEL BERG


Department of Physics and Technology
University of Bergen
Norway

December 16, 2021

# Acknowledgements

The completion of this thesis would not have been possible without my advisor at the Norwegian University of Science and Technology (NTNU), Peter Svensson, who took it upon himself to guide a student from a different university, and share both vast knowledge in and enthusiasm for acoustics. This collaboration would also not have been possible without my advisor at the University of Bergen (UiB), Per Lunde, who suggested reaching out to Svensson in the first place, and helped with all the bureaucratic hoops that had to be jumped through to make it happen. I must also give thanks to Tim Cato Netland, senior engineer at the Department of Electronic Systems at NTNU, for all the help and guidance given during the experimental proceedings of this thesis, not to mention for constructing the objects that were measured on.

I would like to thank my family, for supporting me through all the hardships I have faced, and teaching me to believe I could succeed. You never had a doubt, even though I had plenty. Victoria and Alexander: I love you more than I can express in words.

My friends – you know who you are, and I hope you all know how important you are to me. Lene Svanevik, you have kept my spirits up during the toughest months, and embraced me even at my worst. Caroline Thanh Tran, you are one of the kindest, most courageous people I have ever met. Andreas Handeland and Ingrid Bjørge-Engeland, thank you for keeping me sane in the past months, and for all the laughs in the years I have known you. Lastly, to all my friends in Bergen and beyond: You have made me feel so loved, cared for, and appreciated in the past eight years. I hope I have managed to give back at least a fraction of what you have given me.

Isabel Berg

Bergen, 20.11.21

# Abstract

Uncertainty was estimated for seven variable changes in sound scattering measurements in an anechoic chamber to explore their impact individually and compared to each other. These variables were change of loudspeaker, switching the ventilation system on/off, repositioning the microphone, repositioning the loudspeaker, deviation in velocity of sound, deviation in angle of normal incidence, and deviation in dimensions for the scattering object. This was studied for a cylinder and a box object. For four of the variables the uncertainty was estimated by use of repeated measurements, using post-processing to find the directivity index of the microphone as mounted in the scattering object. Simulations were used to study the latter three, utilizing the analytic solution for an ideal infinitely long, rigid cylinder, while the box was modeled with a numerical solution toolbox which uses the edge source integral equation (ESIE) method.

For the cylinder object, a change in loudspeaker led to a change in directivity index limited to 0.6 dB for most of the $ka$ values. For the variables that were simulated, the difference in directivity index was within a range of $\pm\ 3 \times 10^{-3}$ dB, with a deviation in the velocity of sound contributing most at lower frequencies, while a deviation in the radius of the cylinder gives the largest difference from $ka$ values 10 and above. For the box object, four variable changes were compared through measurements, where the difference in directivity index stayed within a range of 0.5 dB for most frequencies. A change in loudspeaker gives the largest difference for lower frequencies, while for $kl$ values 20 and above, repositioning the microphone and the scattering object gives the largest difference in directivity index. For the simulated variables, the difference in directivity index was found to be less than approximately $\pm$ 0.04 dB; up to $kl$ number 50 the largest contributor is a deviation in the box dimensions, while higher $kl$ numbers saw deviation in the angle of normal incidence having the largest impact. The contribution to the uncertainty for scattering measurements in the anechoic chamber were not all as expected, and for users of anechoic chambers it may be prudent to examine these magnitudes to make sure that the precision is not portrayed as better than what is realistic due to unknown uncertainties.

# List of Symbols

| | |
|---|---|
| $\epsilon_n$ | Neumann factor, value 1 for $n = 0$ and value 2 for $n > 0$, [1] |
| $\phi$ | Circular cylindrical coordinates: Azimuth angle |
| $\rho$ | Circular cylindrical coordinates: Radius of the cylinder |
| $\bar{X}$ | Mean of sample |
| $a$ | Radius of cylinder, [m] |
| $c$ | Velocity of sound, [m/s] |
| $D$ | Measured sound pressure, [Pa] |
| $DI$ | Directivity index, [1] |
| $f$ | Frequency, [Hz] |
| $f_0$ | Cutoff frequency for anechoic chamber, [Hz] |
| $G$ | Input signal (frequency domain) |
| $g$ | Input signal (time domain) |
| $H$ | Transfer function (frequency domain) |
| $h$ | Impulse response (time domain) |
| $H'_n$ | Derivative of Hankel function of order n, [1] |
| $k$ | Wave number, [1/m] |
| $L$ | Wedge depth, [m] |
| $l$ | Length of box, [m] |
| $N(f)$ | Additive noise (frequency domain) |
| $n(t)$ | Additive noise (time domain) |
| $N$ | Number of samples, [1] |
| $p$ | Pressure, [Pa] |
| $P_i$ | Pressure amplitude of incoming wave |
| $Q$ | Directivity factor, [1] |
| $S$ | Standard deviation of the range |

| | |
|---|---|
| $S$ | System output (frequency domain) |
| $s$ | System output (time domain) |
| $S_c$ | Combined standard uncertainty |
| $S_i$ | Standard uncertainty for input quantity no. i |
| $SNR$ | Signal-to-noise ratio, [1] |
| $t$ | Time, [s] |
| $W_N$ | Total noise power |
| $W_S$ | Total signal power |
| $x$ | Cartesian coordinates along x-axis |
| $X_i$ | Measured value of sample no. i |
| $X_k$ | Discrete time Fourier transform |
| $x_n$ | Sample value of sample no. n |
| $x_s$ | Signal (time domain) |
| $y$ | Cartesian coordinates along y-axis |
| $z$ | Cartesian coordinates along z-axis |

# Contents

# Chapter 1

# Introduction

Acoustics can be defined as the science of sound, or more specifically the generation, transmission, and reception of energy in the form of vibrational waves in matter – not only limited to audible sound, but also including frequencies in the infrasound and ultrasound ranges [1–3]. It spans a wide range of disciplines; architectural acoustics, bioacoustics, physical acoustics, musical acoustics, psychoacoustics, electroacoustics, underwater acoustics, speech, and transducer technology, just to mention a few [3, 4]. In this interdisciplinary field, measurements are important [4], and while experiments have historically played a large part in acoustics, it was in the 1800s established "as a science where measurement, observation, and a mathematical approach could lead to significant progress" [5].

Although measurements are a fundamental part of all technology and science [6], the developments in modern day computer technology have paved the way for use of sophisticated simulation software in acoustics. Especially in the field of room acoustics, simulations have an increasing amount of applications [7]. These algorithms are either based on geometrical acoustics where sound is considered as propagating rays, or based on numerical solutions of the wave equation, with well-known methods such as the finite element method (FEM) and the boundary element method (BEM) [8, 9]. The evaluation of these simulations usually come in the form of comparisons to benchmark measurements in corresponding physical environments [8]. So-called round robin tests have been conducted for measurements, simulation software and evaluation procedures [10], where different groups contribute by providing results of different room acoustical simulation algorithms, with input based on the same information from physical rooms where reference measurements have been conducted [7].

Based on such round robin experiments, Brinkmann et al. [8] state that when evaluating simulation software for room acoustics, there must be a plan for how to give a suitable reference for the simulations, in addition to controlling the uncertainties that come with this reference. However, results of such simulation software comparison experiments are often presented graphically, of which an example can be seen in Figure 1.1.

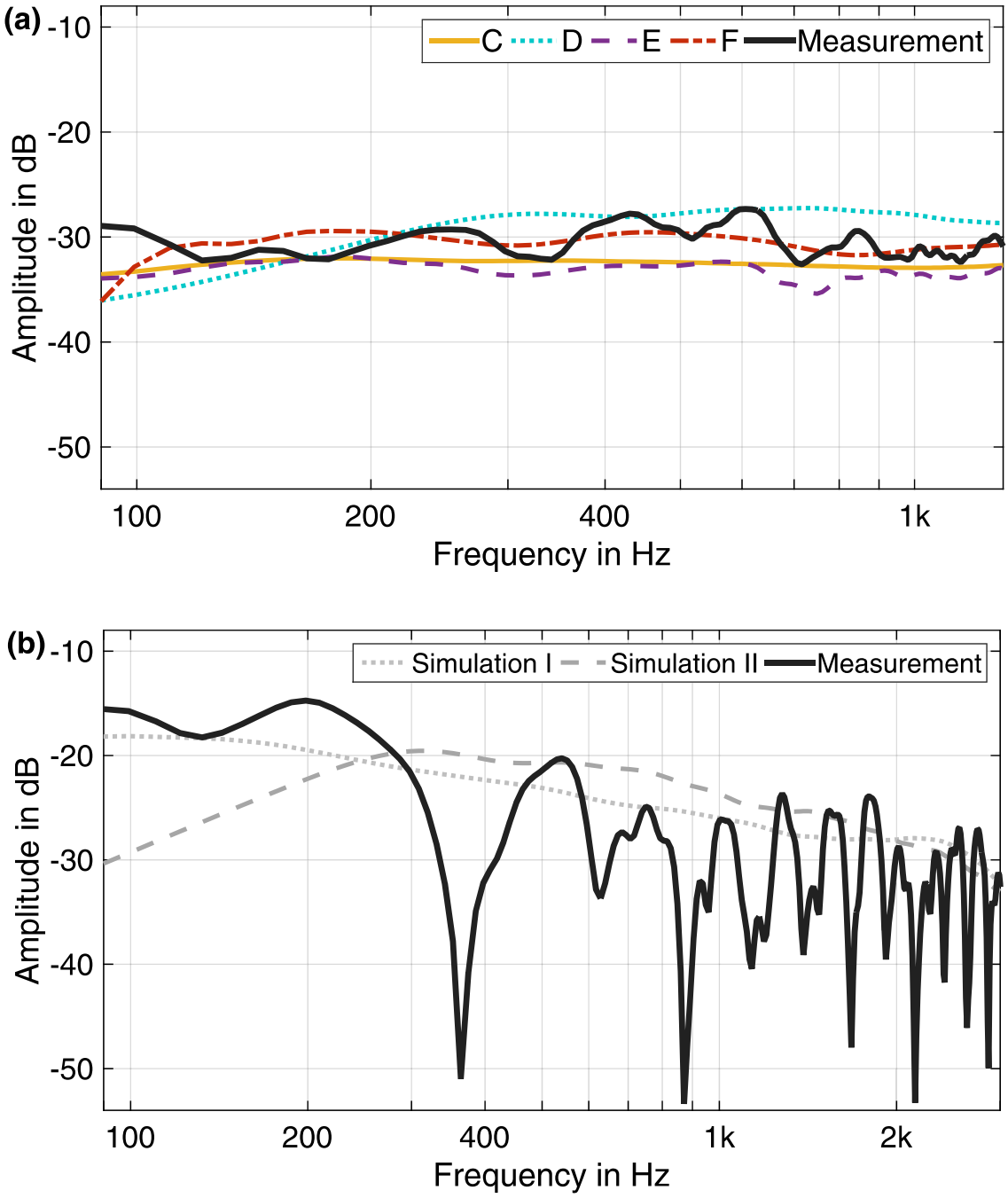


Figure 1.1: The magnitude spectra of measured and simulated impulse responses for grazing incidence at (a) a finite rigid plate, and (b) a quasi infinite wedge. The different simulation algorithms that are participating in the study are anonymized with letters A-F. Some software teams contribute only to selected cases, hence the number of participants differ. From Brinkmann et al. [7], licensed under a Creative Commons License (CC BY).

Figure 1.1 shows the simulated and measured magnitude spectra of the impulse response for grazing incidence for two different objects, with anonymized simulation algorithms. The figure does not, however, give any indication about the uncertainties attached to the reference measurement or the simulations. On the note of simulations, Bork [11] points out that it is difficult to estimate the accuracy of calculation, and that it depends on "numerous parameters not only inherent to the software". Uncertainty is, however, discussed by Brinkmann et al. for measurements, but only for other scenes included in the study, and not the ones illustrated in this figure. Regarding measurements, the *Guide to the expression of uncertainty in measurement* (GUM) by the International Organization for Standardization states that [12]:

> When reporting the result of a measurement of a physical quantity, it is obligatory that some quantitative indication of the quality of the result be given so that those who use it can assess its reliability. Without such an indication, measurement results cannot be compared, either among themselves or with reference values given in a specification or standard.

In other words, estimation of the range of uncertainty for a measured quantity is of equal importance as the determination of the measurement quantity in question [10]. Without addressing the uncertainty of the reference, it is unable to give an accurate evaluation of any simulation. It then becomes impossible to state objectively whether one acoustic simulation software is more accurate than another.

The main motivation behind the work in this thesis is to explore the extent of this uncertainty for measurements of scattering in an anechoic chamber, and to study the range of uncertainties for a selection of variables, for example choice of loudspeaker, and deviation in velocity of sound in air. This is done both through practical experiments and through simple simulations. The experimental work is specific to the anechoic chamber they were performed in, and the overarching goal is not to create a reference measurement, but to gain insight into whether certain variables have a larger influence on measurements than what is initially assumed by users of the anechoic chamber.

Acoustic measurements are often difficult to perform and interpret, and not expected to be absolutely reproducible, with a typical order of 1 dB for deviation in repeated measurements [13]. This is unsurprising, since sound fields and measurement instrumentation is sensitive to minor changes. Hence, while it is of interest to examine the quantitative uncertainty involved in sound scattering measurements performed in an anechoic chamber, and what precision one can achieve with the chosen measurement method, the focus in this thesis is largely on the qualitative result from comparing the impact of the selected variables.

Chapter 2 begins with an introduction to the theoretical background of the topics explored in this thesis, followed by Chapter 3, which describes the methodology of the work, both experimental work and simulations. Chapter 4 details and discusses the results, followed by a conclusion in Chapter 5. Included in the final chapter is also a note about possible future work.

# Chapter 2

# Theory

In this chapter, the theoretical background for the work performed in this thesis will be presented. This includes an overview of the acoustical background, as well as the acoustic signal processing elements that are relevant for the post-processing that has been performed on the measurement data, ultimately affecting the uncertainty of the measurement results.

## 2.1 Scattering

The propagation of acoustic waves are explored extensively in literature, and the fundamentals will not be elaborated on here. The interested reader as well as readers without background in acoustics can see works by Kinsler et al. [1] or Beranek and Mellow [14] for an introduction. Upon delving into the behavior of acoustic waves, a fundamental concept is that of scattering. This describes the phenomenon which occurs when a sound wave encounters an obstacle or an inhomogeneity in the medium it travels through on its path of propagation; in this situation, part of the wave will break off into secondary waves that spread into different directions [15]. Notably, high frequencies scatter much more than low frequencies [2], where "high frequencies" imply that the wavelength of the acoustic wave is much shorter than the dimensions of the obstacle, while "low frequencies" mean that the wavelength is much longer than the dimensions of the obstacle.

Morse [16] defines the scattered wave as the difference between the actual wave and the undisturbed wave. Then, in the case of a wavelength much smaller than the obstacle, half of the incoming wave will spread out somewhat uniformly in all directions, while the other half will interfere destructively with the undisturbed wave at the back of the obstacle and form a clear shadow. However, in the case of a wavelength much larger than the obstacle, which is often the case for acoustic waves, all of the scattered wave will spread out in all directions, and no clear shadow will form. Finally, in cases where the wavelength and obstacle are of comparable sizes, various interference effects can arise. [16, 17]

### 2.1.1 Edge diffraction

A sub-section of scattering is the phenomenon of diffraction [14], which is the ability of a wave to bend around a solid object [18]. This process affects both the amplitude and the phase of the wave involved, dependent on both the frequency and direction of the wave [19]. This bending of the wave allows sound to enter shadow zones [3], which explains why sound can be heard around a corner, despite the inability to see around a corner [18]. This also means diffraction around the edges of objects that are under testing must be taken into account when modeling the behavior of sound waves.

Although not elaborated upon here, the sharpness of the edge, when seen in light of the incident angle of the incoming sound, also affects the resultant scattering or diffraction behavior. This contributes to the difference in analysis of the cylinder and the box objects, as will be seen shortly.

### 2.1.2 Scattering by a cylinder

When the scattering body is a circular cylinder, it is common to use circular cylindrical coordinates for expressing waves. These coordinates $(\rho, \phi, z)$ are related to Cartesian coordinates $(x, y, z)$ by the following transformation [20]:

$$\begin{aligned} x &= \rho \cos \phi \\ y &= \rho \sin \phi \\ z &= z \end{aligned} \tag{2.1}$$

where $\rho$ is the radius of the cylinder, and $\phi$ is the azimuth angle.

Circular cylinders have a simple geometry, and have been studied thoroughly, for instance by Bowman et al. [20]. Due to its geometry, mathematical expressions exist that describe its scattering behavior. The ideal case of an infinitely long, rigid cylinder was first solved by Morse with some wavelength limitations [21], but analytical solutions of various forms without such limitations can be found in several literary works, including Morse and Ingard [17], Rhee and Park [22], and Junger and Feit [23]. The equation written in the format used by Junger and Feit is shown below, giving the pressure at a point on the surface of the cylinder for an incoming plane wave propagating along the negative x-axis:

$$p\left(a, \phi\right) = \frac{2P_i}{\pi k a} \sum_{n=0}^{\infty} \frac{\epsilon_n j^{\,(n+1)}}{H_n'(ka)} \cos\left(n\phi\right) \tag{2.2}$$

where $p\left(a, \phi\right)$ is the pressure in a point at distance $a$ from the centre of the cylinder, with $a$ being the radius of the cylinder. $P_i$ is the pressure amplitude of the incoming plane wave, and $k$ is the wave number, equal to $(2\pi f)/c$ where $f$ is the frequency in hertz and $c$ is the velocity of sound. $\epsilon_n$ is the Neumann factor, which has value 1 for $n = 0$ and 2 for $n > 0$ [24]. Lastly, $H_n'$ is the derivative of the Hankel function of order $n$; a Hankel function is a linear combination of two Bessel functions [25].

The mathematical aspect of the Bessel functions, and hence the Hankel function, will

not be elaborated upon here. The interested reader could see Watson [26] for an in-depth study of this, while a short introduction can be found in Appendix D of the work by Lamb Jr. [27]. Modern programming platforms tend to have built-in functions for this. While a function exists in MATLAB for the Hankel function, the derivative does not. In order to express the derivative of the Hankel function, the following equation can be used [28]:

$$\frac{d}{dz} H_n^{(1)} = \frac{nH_n^{(1)}(z)}{z} - H_{n+1}^{(1)}(z) \tag{2.3}$$

where the superscript (1) indicates a Hankel function of the first kind, $n$ is the order of the Hankel function, and $z$ is the argument the Hankel function takes in.

It is noteworthy that in Equation 2.2, the argument that the Hankel function takes as input is the dimensionless quantity $ka$, consisting of the wave number and the radius of the cylinder. This quantity is often used as a variable for expressing frequency dependency rather than simply using the frequency value in hertz. Given the definition of the wave number as given after Equation 2.2, the $ka$ number can be defined as:

$$ka = \frac{2\pi f a}{c} \tag{2.4}$$

It should also be mentioned that while the analytical solution exists, the sum in Equation 2.2 goes to infinity. When using this equation for calculations, the sum is truncated. The exact number of elements that are included is decided by testing when this sum begins to converge, meaning when adding the next element in the series does not change the value of the sum above a certain precision. This will be specified in Chapter 3.

### 2.1.3 Scattering by a box

Equations have only been solved exactly for a few simple scattering shapes, which are cases where the wave equation is separable [20, 29]. This does not include the complex shapes of cubes or rectangular boxes. For these cases, numerical solutions can be found through established methods such as the Boundary Element Method (BEM) or the Finite Element Method (FEM), although these are computationally heavy [29, 30]. More recently, an alternative method has been developed, known as the edge source integral equation (ESIE). This models scattering by convex, rigid bodies by use of an edge diffraction-based approach [9].

ESIE does, however, have some numerical challenges, which are overcome by combining the edge source integral equation with the boundary element method, producing a proposed method with the notation ESIEBEM [31]. The interested reader may see the work by Martin et al. [31] for details about this method.

In order to reach such a numerical solution, it is possible to use the toolbox known as "EDtoolbox", which is MATLAB-based and was developed by Svensson [32]. This toolbox calculates the sound pressure for a scattering object with rigid surfaces, given that it is an external scattering problem, using either the ESIE or the ESIEBEM method.

More details can be found in the manual of the toolbox, which is published at GitHub. [32]

As was noted for the cylinder, it is common to present results that are a function of frequency by use of the dimensionless $ka$ number. Boxes, however, do not have a radius. An alternative is to use the length of the box instead, which results in a $kl$ number, where $l$ is the length of the box. An example of this being used can be found in the work by Skelton [29], where different frequency regions for the resulting scattering on a two-dimensional rectangle are compared (p. 1770). Equivalently to Equation 2.4, the $kl$ number can be defined as:

$$kl = \frac{2\pi f l}{c} \tag{2.5}$$

### 2.1.4 Reciprocity

For acoustic measurements, a commonly used concept is that of reciprocity. Simply put, the principle of acoustic reciprocity states that if a pair of a small source and a small receiver are interchanged in an environment that remains unchanged, then the received signal will be identical [1]. In other words, the pressure which is measured at a point A originating from the signal of a source at point B, is equal to that measured in point B with the source at point A if the system is subjected to no further changes [17].

Morse and Ingard [17] used reciprocity to explain that the pressure at the surface of a cylinder is the same as that at some distance from the cylinder due to a vibrating line element. In this thesis, it clarifies the exchange of loudspeaker and microphone positions during measurements. This will be further discussed in Section 2.1.5.

### 2.1.5 Directivity

For the sake of doing practical measurements of how sound is scattered by an object, one would be interested in how the sound pressure level would vary around the object in different directions. As a parallel, many sound sources also exhibit a property known as directionality, which is when the sound pressure level at a certain distance is not equal in all directions [5]. The change in level depending on the direction of the source is known as directivity, and one commonly distinguishes between the horizontal and vertical patterns of directivity [5]. Here, the focus will be on the horizontal directivity.

Taking the cylinder as an example, the combination of a scattering object with a loudspeaker mounted on its surface could then be considered as a loudspeaker unit, and its directivity could subsequently be studied. To measure this, one would place a receiver in several positions around the cylinder, and measure how the perceived pressure varies with the angle. Due to reciprocity, however, it is possible to do the opposite: to place a receiver at the cylinder, and a loudspeaker in several different positions around the cylinder.

One loudspeaker could then be rotated around the cylinder. However, the measurements

would be identical regardless of whether the loudspeaker rotated around the cylinder, or the loudspeaker was stationary and the cylinder rotated instead. This is the basis of the measurement procedure that has been performed in an anechoic chamber.

### Directivity factor

A quantity to describe the directivity is the directivity factor. This is the ratio between the intensity at a given distance on a chosen reference axis and the averaged intensity emitted by the same loudspeaker in all directions [3, 14]. This can be summarized by the following equation [33]:

$$Q = \frac{|D|^2_{ref}}{< |D|^2 >} \tag{2.6}$$

where $D^2_{ref}$ is the response caused by sound coming from the reference direction, typically $\phi = 0$ (normal incidence), while $< |D|^2 >$ is the response found by averaging the responses from all possible angles of incidence. As intensity is proportional with the sound pressure squared, $D$ represents the measured sound pressure, while the squared quantities represent intensities.

In the horizontal plane, and with measurements performed in a finite number of angles, Beranek and Mellow [14] propose an expression for the directivity factor as a function of frequency, where they weight the measured root mean squared (RMS) values of the sound pressure at normal incidence divided by a sum of all the measured angles. In their expression, the weights are dependent on measuring only between 0° and 180° and the sound source assumed to be symmetrical. However, they comment that in the event of a non-symmetrical directivity pattern, this can be modified to suit measurements for the full range of 0° to 360°, effectively averaging the two sides of the directivity pattern [14].

### Directivity index

After having calculated the directivity factor for different frequencies, one can plot the directivity index in decibels as a function of frequency. The directivity index is calculated from the directivity factor as follows [14]:

$$DI(f) = 10 \log_{10} Q(f) \quad [\text{dB}] \tag{2.7}$$

where $DI(f)$ signifies that the directivity index is a function of frequency, since the directivity factor $Q(f)$ is a function of frequency.

## 2.2 Anechoic chamber

When measuring scattering on an object with the purpose of studying that particular object's behavior, it would be preferable for the measurements not to be affected by reflections from surfaces of the surroundings. If there are no reflections from the surroundings, then it would be equivalent to the free-field condition: sound propagates as it would freely in the atmosphere [34]. This condition occurs naturally in an open outdoor space, if sufficiently far removed from the Earth's surface [35].

In order to achieve this indoors, the surfaces of a room must be covered in sound-absorbing material, where porous material shaped into wedges are most commonly used [36, 37]. There are other conditions factoring into whether an acoustic room can be qualified as fully anechoic or not, where procedures described in ISO3745 and ISO26101 are used for qualification [35]. However, in essence, these rooms provide a controlled environment without reflections and unwanted signals from outside the chamber [38].

### 2.2.1 Cutoff frequency

While wedges designed for use in an anechoic chamber tend to have a large absorption at high and medium frequencies (larger than 300 Hz) [37], the limitation is usually at the lower frequencies, which is expressed by the low frequency cutoff $f_0$. This is defined as the lowest frequency at which the room can have anechoic behavior [36], meaning an absorption coefficient for the surface of the room larger than 0.99 [34]. This cutoff frequency can be approximated by the following theoretical formula [36]:

$$f_0 = \frac{c}{4\,L} \tag{2.8}$$

where $f_0$ is the cutoff frequency, $c$ is the velocity of sound in the chamber, and $L$ is the depth of the wedges covering the surfaces of the room. While the cutoff frequency is determined experimentally according to ISO3745 [34], this simple theoretical formula gives an estimate of the lower limits for measurements that can be done in a given anechoic chamber.

## 2.3 Acoustic signal processing

This section describes the processing of the measurements performed in the anechoic chamber in order to find the directivity index. During the measurement procedure a microphone converts sound waves in air to electric signals [39], the electric signals are sampled and quantized (i.e. digitized) by the analog-to-digital converter, and the digital signals are interpreted by the measuring software to produce the impulse response [40]. The Fourier transformation of this impulse response produces a transfer function representing the system behavior [40], as will be elaborated upon below.

### 2.3.1 System description

A measurement system can be described as the link between a process which generates information and the observer to the process [6]. The scattering of sound by a scattering object in the anechoic chamber can then be seen as a process, and in combination with the presence of a microphone measuring the sound waves, which is later processed and presented, this can be termed the measurement system. The input of the system is then the real sound waves generated by the scattering, while the output of the system is the measured value, which in this case is a discretized impulse response as generated by the measurement software.

#### Frequency domain

A linear and time-invariant (LTI) system can be identified in time entirely by the relationship between its input and output [41]. Linearity refers to the system behavior being invariant regardless of changes in input power [13]. Alternatively, linearity can be interpreted as the system obeying the principle of superposition [42]. The property of time-invariance indicates that the characteristics of the system remain fixed with time [42].

The relationship between the input and the output of a system is known as the system behavior. This can be represented by the impulse response or the transfer function, depending on whether it is expressed as a function of time or frequency; functions of time are said to be in the time domain, while functions of frequency are in the frequency domain. The system behavior is illustrated in the block diagram in Figure 2.1. It can also be represented by a convolution in the time domain, or a multiplication in the frequency domain, as shown below [10]:

$$\begin{aligned} g(t) &= s(t) \ * \ h(t) \\ G(f) &= S(f) \ \bullet \ H(f) \end{aligned} \tag{2.9}$$

where $t$ denotes a function of time in the time domain, and $f$ denotes a function of frequency in the frequency domain, $s(t)$ and $S(f)$ is the input signal, $g(t)$ and $G(f)$ is the system output, $h(t)$ is the impulse response and $H(f)$ is the transfer function.

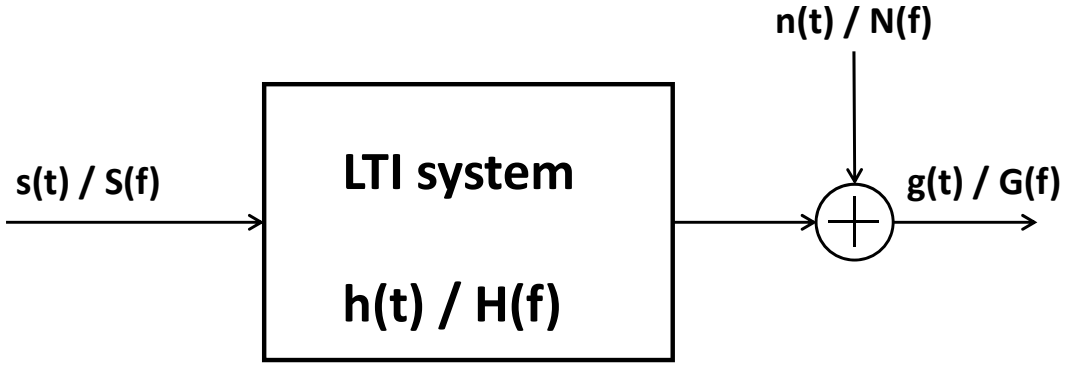


Figure 2.1: Block diagram of an LTI system with descriptions in the time and frequency domains. The input signal s(t) or S(f) and the system output g(t) or G(f), with the impulse response h(t) or transfer function H(f) and the additive noise n(t) or N(f). The noise can be both acoustic and electric. Recreated from Fig. 3.1 in the work by Dietrich [10], and Fig. 1 in the work by Farina [43].

### Fourier transform

Given that the system is linear and time-invariant, the impulse response can be transformed into the frequency domain [13, 44]. The transformation between the time domain and the frequency domain is done by use of the discrete time Fourier transform [45]. While the real signal of sound waves is analog and continuous, the signal processing requires this to be digitized. The signal is sampled in time and quantized in value, thus converting it to a discrete-time signal [46]. If a signal is sampled at every $T = 1/f_s$ with $T$ being the sampling period, and $f_s$ being the sampling frequency, then evaluating the Fourier transform at frequencies $f = k/T$ for $k = 0, 1, 2, ..., N-1$ for a total of $N$ samples, the following discrete Fourier transform (DFT) is produced [46, 47]:

$$X_k = \mathcal{F}\left\{x_s(t)\right\} = \sum_{n=0}^{N-1} x_n \, e^{-j2\pi kn/N} \tag{2.10}$$

where $X_k$ is the discrete time Fourier transform of the signal $x_s(t)$, which is represented by the sample value $x_n$ for a total number of samples $N$, evaluated for all frequencies $k$ which the frequency spectrum is made up of. The mathematical background of the Fourier transform is explored in several literary works, and will not be elaborated upon here. The interested reader can consult the work by Kido [47]. In general, the discrete Fourier transform can be interpreted as relating a sampled time signal to a sampled spectrum [4].

Further, the computation of the discrete Fourier transform can be made more efficient by use of the Fast Fourier transform (FFT) algorithm, which reduces the number of operations by grouping terms [47, 48]. The most efficient FFT algorithm is used when the sample size of the signal is a power of 2, which reduces the number of multiplications needed [48, 49]. This gives rise to the use of zero padding, which is when the sample is

extended by values of zero to achieve a certain length [49].

### 2.3.2 Impulse response measurements

With the system behavior being represented by the impulse response or transfer function, certain precautions must be made. Firstly, which stimulus signal to utilize is an important choice. One must also ensure that the system response is not too masked in noise. Lastly is the post-processing done to the system response when using the discrete time Fourier transform to find the transfer function. In this process, a window function needs to be used to extract only the direct sound for further analysis.

#### Impulse response

The EASERA measurement software generates a stimulus signal when used to measure impulse response. The stimulus signal used here is a logarithmic sweep, which is elaborated upon shortly. The system response, as recorded by the microphone, is a combination of the stimulus signal and the system behavior; when eliminating the stimulus signal one is left with the system behavior, which is represented by the impulse response [40].

#### Logarithmic sweep

There are different stimulus signals that can be used. One of those is the sweep; the system is driven by a sinusoidal signal with a frequency that is slowly increased to sweep through the frequency range of interest [4]. Sweeps can have different designs, for example linear and logarithmic. Linear sweeps, where the frequency increases linearly per time interval, are said to have white coloration, while a logarithmic sweep, where the frequency doubles per time interval, is known as a pink excitation signal [40, 50]. Upon comparison, the logarithmic sweep gives a stronger signal at lower frequencies due to sweeping more slowly there and faster at high frequencies [43, 45]. Hence, for the measurements in the anechoic chamber, a logarithmic sine-sweep will be utilized.

#### Signal-to-noise ratio

Keeping in mind that the system is assumed to be linear and time-invariant, the output registered by the receiver will be signal and the noise added together [51], as illustrated in Figure 2.1. For the sake of quantifying how contaminated the signal is with acoustic and electric additive noise, a useful quantity is the signal-to-noise ratio (SNR), which is defined as the ratio of signal power to noise power [51]. This is often expressed in decibel, with power values as [6]:

$$SNR = 10 \log_{10} \left( \frac{W_S}{W_N} \right) \text{ [dB]} \tag{2.11}$$

where $W_S$ is the total signal power and $W_N$ is the total noise power, with signal power being proportional to the signal squared. The quantity in Equation 2.11 could be

expressed with RMS values by replacing $10 \log_{10}$ with $20 \log_{10}$ [6].

In the experimental situation, this noise cannot be turned off in order to measure the signal alone; instead, the signal must be switched off and the noise measured by itself, and the signal measured along with noise [51]. The measured signal-to-noise ratio can then be expressed by:

$$SNR_{meas} = 10 \log_{10} \left( \frac{W_S + W_N}{W_N} \right) \text{ [dB]} \tag{2.12}$$

Comparing Equation 2.12 to Equation 2.11, the true value of the SNR can then be expressed by the measured SNR as follows:

$$SNR_{true} = 10 \log_{10} \left( 10^{SNR_{meas}/10} - 1 \right) \text{ [dB]} \tag{2.13}$$

### Windowing

When analysing the system response to find the system behavior, the goal is to find the result of the scattering process on the scattering object. With this in mind, only the direct sound and how it is scattered is of interest – reflections, for instance on the mounting of the object, the turntable, or on other surfaces in the measurement setup, do not provide information about how sound is scattered by the object under testing. For this reason, the measured impulse response, which extends for several seconds, is windowed around the relevant part of the impulse response. The purpose of a time window here is to extract a smaller portion of a sample sequence [47].

Several different time windows see use in signal processing. In this work, the Hanning window was utilized, which is a tapered window using a sine function for constructing the tapering and is one of the most common windows used in frequency analysis applications [47]. More specifically, the used window is a half-Hanning window, where the first half is in effect a rectangular window, while the latter half has tapering which de-emphasizes data near the edge of the window [46]. Due to the nature of the anechoic chamber, this approach is deemed safe as there are no unwanted reflections before the excitation signal begins: the beginning of the direct sound is clearly defined in the impulse response. The specifics of the utilized window function's design is described in Section 3.1.5.

## 2.4 Uncertainty

Literature on the concept of uncertainty has traditionally been dominated by the terms "true value" and "error" [12]. For instance, Bentley [6] defines the measurement error as the difference between the measurement value and the true value, and states that accuracy is the closeness of the measured value to the true value. The ISO standard 98-3:2008 called *Guide to the expression of uncertainty in measurement* [12], however, avoids using these terms, instead presenting the same concepts by use of the measured result and its evaluated uncertainty, where the particular quantity subject to measurement is known as the measurand.

ISO 98-3:2008 states that there are several interpretations possible for the concept of the uncertainty of a measurement, both as a measure of possible error in the estimated value for a measurand, and as an estimate for the range of values which the true value of a measurand lies within. Here it will be used in the sense of the latter. The standard also states that a result of a measurement is merely an estimate of the value of the measurand, and is only complete when associated with an uncertainty of the estimate. There are different ways to evaluate uncertainty components; one option is the estimated standard deviation, which is calculated from repeated observations. The best estimate of the measurand from these repeated observations may then be the arithmetic mean of the observations. When the uncertainty of the result is expressed as a standard deviation, it is referred to as the standard uncertainty. [12]

### 2.4.1 Sample mean and standard deviation

The mean of several measurements performed on the same quantity can be calculated by use of Equation 2.14 [52].

$$\bar{X} = \frac{1}{N} \sum_{i=1}^{N} X_i \tag{2.14}$$

where $\bar{X}$ is the sample mean, $X_i$ is the measured value of sample no. $i$, and $N$ is the number of samples.

The uncertainty from the range of these measurements can then be described by the standard deviation of the range, as given in Equation 2.15 [52].

$$S = \sqrt{\frac{\sum_{i=1}^{N} \left(X_i - \bar{X}\right)^2}{(N-1)}} \tag{2.15}$$

where $S$ is the standard deviation of the range.

### 2.4.2 Combined standard uncertainty

When several quantities are combined to form a result, the standard uncertainty of the result is calculated by finding the positive square root of a sum of terms, which can be expressed as follows [12]:

$$S_C(y) = \sqrt{\left(\sum_{i=1}^{N} S_i^2(y)\right)} \tag{2.16}$$

where $S_C$ is the combined standard uncertainty for an estimate $y$, and $S_i$ are the standard uncertainties of the different independent input quantities.

## 2.5 Sources of uncertainty

Following is a discussion of various sources of uncertainty that are considered for the experimental data. Sources of uncertainty for the simulations are beyond the scope of this thesis, and will not be elaborated upon here. In the event of comparison between simulated results and experimentally acquired results this would be necessary to include, but in this work the simulations are performed mainly with the purpose of learning about the magnitude of uncertainty originating from the sources that are studied, and not for comparing the measured and simulated directivity index.

### 2.5.1 Velocity of sound

For electromagnetic waves, Expósito et al. [38] state that environmental conditions, such as humidity and temperature, have an influence on the wave propagation inside the chamber, and on the measurement instrumentation. They further state that for their study of uncertainty in measurements of the parameters of antenna in an anechoic chamber, the magnitude of the uncertainty of these environmental conditions were negligible compared to other sources of uncertainty. This work will explore whether this is also the case for acoustic waves.

In addition to the humidity and temperature, air pressure also affects wave propagation, due to its correlation with the velocity of sound. During the processing of the measured data, measurements of these environmental conditions are used to estimate the velocity of sound, by use of relationships in the work by Rasmussen [53]. These relationships have been implemented in a MATLAB script called "amb2prop" by Dr. Vicente Cutanda Henriquez at the Technical University of Denmark. The script is included in the package "OpenBEM" [54]. For these measurements it should be noted that a barometer with an analog display was used to monitor the air pressure, and personal bias may occur in reading of such instruments [12].

### 2.5.2 Position

As transfer functions are unique for the measurement system, differences in the position of the elements involved will affect the resulting estimate of the measurand. With the measurand being sound pressure, it is noteworthy that Doebelin [55] states that pressure is not a fundamental quantity, but derived from force and area, which again are derived from mass, length and time. Even more notably for the measurement of sound pressure in relation to scattering behavior is that changes in position may affect the scattering pattern itself. Consequentially, in typical sound scattering measurements, the elements in the measurement setup are mounted in specific positions relative to each other, and these mounted positions will have an associated uncertainty. For this reason, one might assume position to be one of the largest contributors to uncertainty for the measurements explored in the work of this thesis.

### 2.5.3 Transducer properties

The loudspeakers and microphone used will potentially add to the uncertainty in the estimate of the measurand. One aspect is the physical limitations of the transducers, based on the range of frequencies they can operate in due to size and construction, but an additional element is the possible directivity of these transducers. A directional source (or receiver) will cause deviations in the scattered field compared to a hypothetical point source [56], causing an even larger effect from uncertainty in position. Hence, the directionality of loudspeakers and microphones causes their orientation to be of importance. The microphone is also rotated through a full revolution of measurements, making microphone directivity an important factor. For the type of microphone used, the directivity is known to increase for increasing frequencies [57].

Though non-linear behavior is not given much attention in this work, it should be mentioned that loudspeakers and microphones may behave non-linearly outside of their recommended frequency range. Additionally, ageing is an important contributor to transducers not behaving as expected, which should be taken into account when discussing results obtained experimentally.

### 2.5.4 Ambient noise

Of note is also the fact that random noise on the measurement site will affect the measurements that are performed. One known source of such random noise is the ventilation system. Duanqi et al. [37] states that it is both necessary and possible to have a ventilation system condition the air in the chamber, but that the challenge is to achieve the right attenuation to avoid noise from outdoors reaching the inside of the chamber. In order to eliminate the ambient noise due to the ventilation system, one could simply switch it off while performing measurements inside the chamber, accepting that the environmental conditions would change slowly but surely as the air in the chamber is no longer being conditioned.

Despite anechoic chambers being built to eliminate reflections, there is still ambient noise present in the chamber, albeit to a lesser extent compared to normal rooms. Due to the presence of random noise, a measurement of the sound level emitted in the room with no stimulus signal present gives an indication of the noise floor. Combining this with the expression for the signal-to-noise ratio, one can identify the regions where the system response is not too masked in noise to be extracted. In other words, it is possible to identify regions of the measurement interval where the estimated value for the measurand are deemed reliable above some chosen precision.

### 2.5.5 Processing

There are several different factors that can contribute to uncertainty while processing the measured data. Though not within the main scope of the work in this thesis, parts will be taken into account during the discussions found in Chapter 4. These factors are the effect of the window size used when performing the discrete Fourier

transform, the placement of the starting and ending point of the window, and the mismatch when comparing curves with different x-values. Other aspects of uncertainty and error introduced by post-processing of the measured data can be read about in most works about digital signal processing.

### 2.5.6 Miscellaneous

There are numerous other sources that may contribute to the uncertainty in the estimated value of the measurand. The analog-to-digital and digital-to-analog converters introduce errors, but these can be expected to be much smaller than many other sources due to the high precision of the instruments used. It should also be mentioned that there may be other unacknowledged errors based mostly on the skill and expertise of the person running the experiment [56].

The sources of uncertainty mentioned here are not exhaustive, but merely an indication of the main points that are kept in mind throughout the experimental work. As stated in ISO 98-3:2008, the value of the measurand may never be known exactly, only the estimated value can be known, and the uncertainty is an expression of how there is not one value but an infinite number of values distributed around the result that are consistent with all observations, data, and one's knowledge of the physical world [12]. To summarize, there may always be unrecognized sources of uncertainty, and one may never know the error in the measurement result. With that said, when expressing an estimate for a measurand based on measurements, we are also responsible for expressing our certainty in this estimate based on available knowledge.

# Chapter 3

# Methodology

The practical aspect of the work that forms the basis for this master's thesis was divided into two main aspects: experimental measurements of sound scattering on an object in an anechoic chamber, and simulations of the experimental situation. Further, measurements and simulations were performed for two different scattering objects, namely a cylinder and a box. These two objects were chosen based on what would be practically possible to build and perform measurements on within a reasonable time frame, while additionally keeping in mind how simulations could be performed. The simulations were done in MATLAB, using the analytical solution for scattering by an infinitely long cylinder, while simulations for the box were done using a toolbox for edge diffraction, called EDtoolbox. Simulations were performed mainly for the purpose of estimating the effect of a deviation in some parameters, such as the velocity of sound. The scripts written for use in this thesis can be found at GitHub [58].

Experimental measurements were performed with the objective of quantifying the uncertainty caused by different influences. They were carried out at the newly restored anechoic chamber at the Faculty of Information Technology and Electrical Engineering at the Norwegian University of Science and Technology (NTNU), with both objects to be measured on being constructed by the workshop at the Department of Electronic Systems. As for what unit to measure, it was decided to measure a relative unit, so that the calibration required for absolute measurements would not be necessary. For this purpose, a horizontal-plane directivity factor and its corresponding directivity index were deemed practicable. Note that the use of the term "directivity factor" here is not standard. The background for this can be found in Section 2.1.5.

## 3.1 Measurements

Following is a description of the process of completing experimental measurements on a constructed cylinder and box object, including the build of the objects, how they were installed in the anechoic chamber, how the electrical setup was connected, and how the measurements were practically performed.

### 3.1.1 Construction and setup

The cylinder object to be measured on was constructed out of a PVC pipe, with a length of approximately 3.6 m. The pipe was divided in two parts, and a hole was drilled into the side so a microphone with a pre-amplifier could be mounted on the pipe, whilst simultaneously maintaining the smoothness of the surface. Hence, the effect of the microphone on the scattering on the pipe was limited. The pipe was then filled with absorbant material to limit the effects of any internal resonances, and the two parts were fitted around a hard plastic connector, maintaining the smooth surface. The upper end was closed with another piece of hard plastic, with a hole on the top to allow for mounting on the steel rods installed in the roof of the anechoic chamber, thus securing the object from wobbling due to its length. In the end of the lower half, a rod was installed so it would be possible to securely position the pipe on the turntable. A photograph of the pipe post-installation in the anechoic chamber, with a magnified cutout of the microphone mounted in the surface of the pipe can be seen in Figure 3.1. The dimensions of the completed pipe were measured, and can be found in Table A.1 in Appendix A.

The box element was built from wooden elements, with a thickness of approximately 15.3 mm. The inside was lined with absorbant material, while the center remained hollow. The front plate had three different holes drilled into it to make room for different microphone placements. The center placement was utilized for this experiment, while the others were filled with metal plugs screwed in to maintain a smooth surface. The microphone was connected to a pre-amplifier, and the cord came through a hole in the back of the object, sealed with absorbant material. The box was installed on top of a metal rod with a pedestal, which was secured into the turntable. The box object as placed in the anechoic chamber can be seen in Figure 3.2, including a magnified cut of the surface of the constructed object. The dimensions of the completed box were between 35 and 40 cm, with a slightly rectangular build. The measured dimensions can be found in Table A.2 in Appendix A, along with an illustration of the indexing of said dimensions in Figure A.1.

When installed in the anechoic chamber, the cylinder object was mounted both in the ceiling and on the turntable, and the microphone with its pre-amplifier was connected to another amplifier, which subsequently connected to an Analog-to-digital converter (ADC) through a connection rail. The ADC unit then connected to a computer for the signal to be recorded. The loudspeaker was installed at the same height as the microphone by use of a laser level. The speaker received its signal through a Digital-to-analog converter (DAC), connected to a power amplifier, and lastly connected to the speaker through the connection rail. A diagram of the measurement setup is given in Figure 3.3. The equipment used during the sound scattering measurements is listed in Table A.3 in Appendix A. For the cylinder, there was not a barometer present in the anechoic chamber. The box object was mounted on top of a steel plate, with an attached steel rod that was fastened into the turntable. The measurement setup was similar to the setup for the cylinder (Figure 3.3) with the addition of a web camera

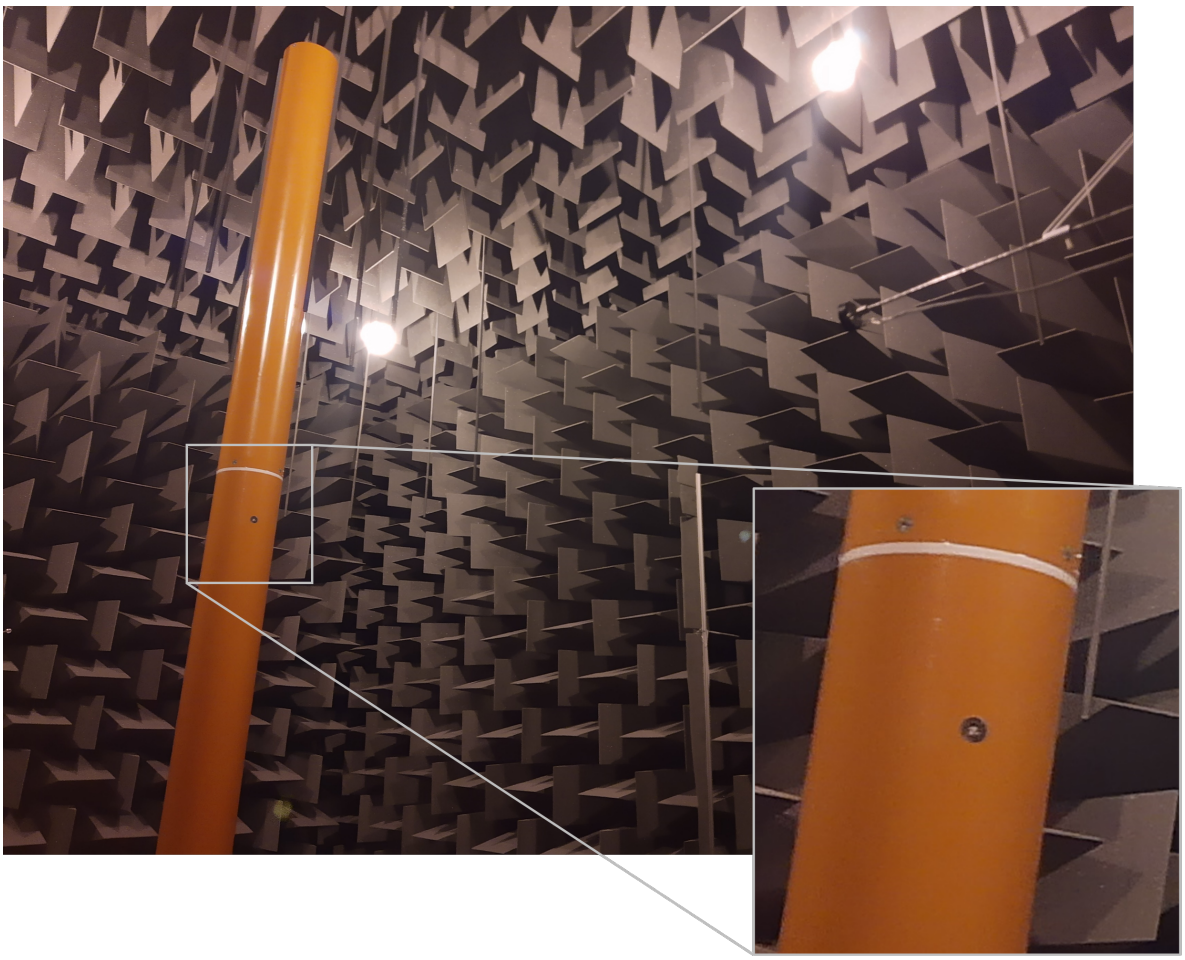

Figure 3.1: Photograph of the constructed cylinder object mounted in the anechoic chamber, with a magnified cutout of the microphone installed at the surface of the pipe. To the right one can see the speaker which will be labeled as speaker #1.

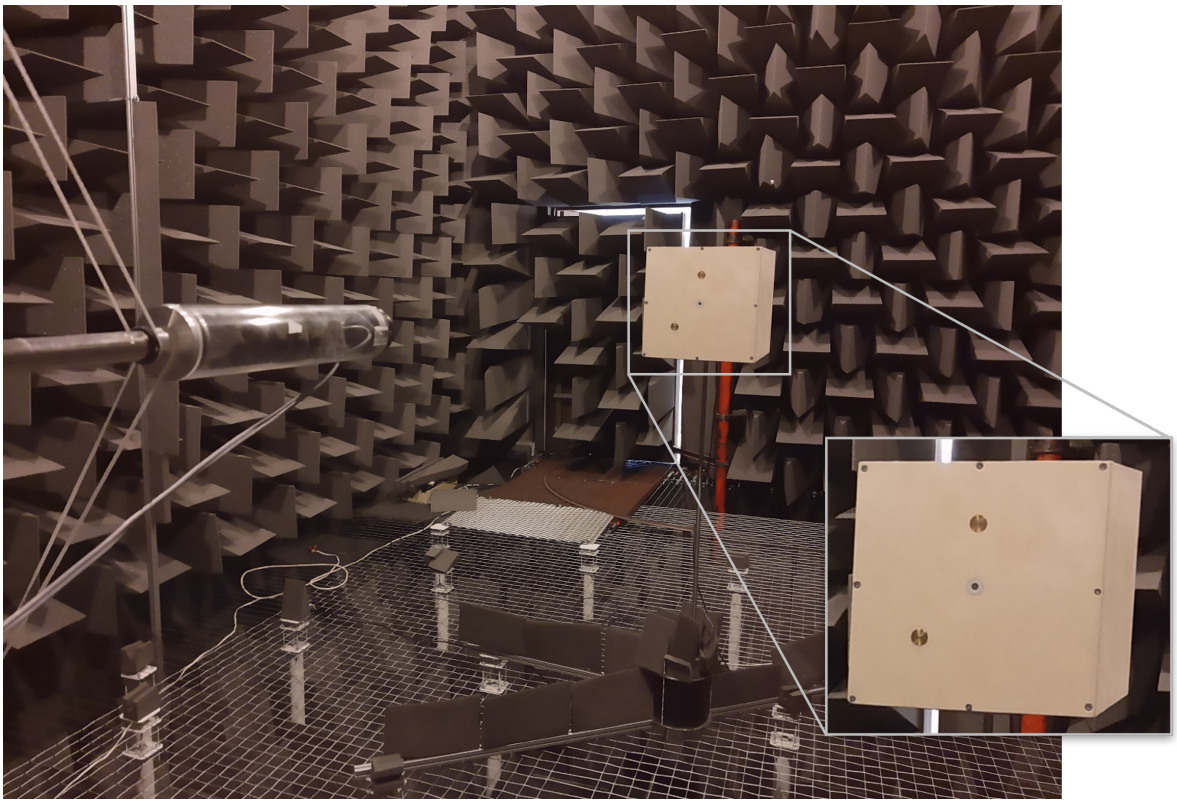

Figure 3.2: Photograph of the constructed box object mounted in the anechoic chamber, with a magnified cutout of the microphone installed at the surface of the box. To the left one can see the speaker which will be labeled as speaker #2.

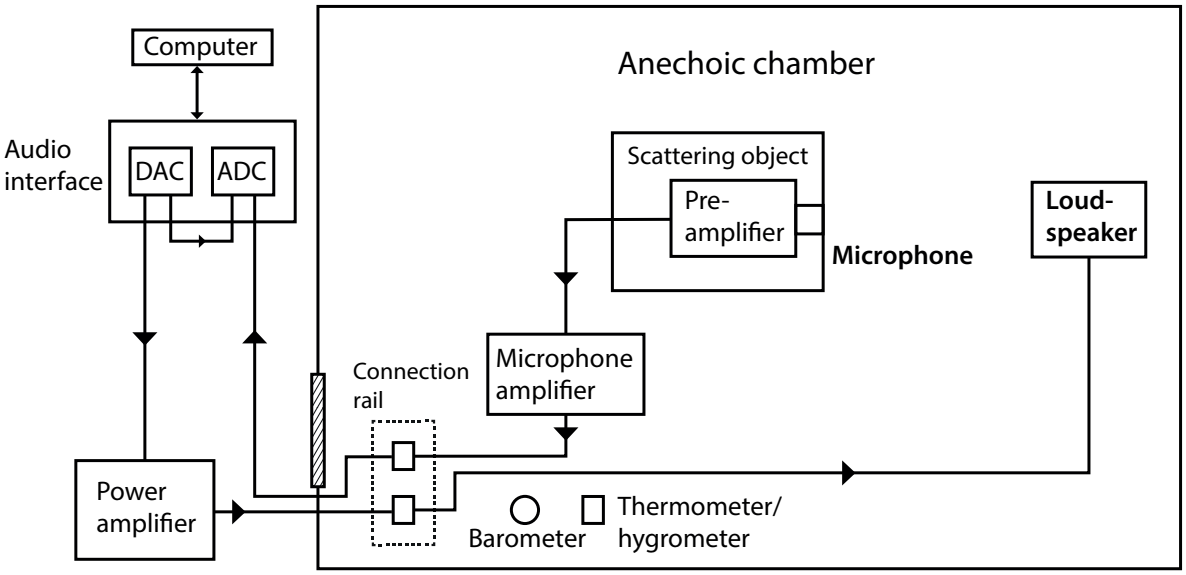


Figure 3.3: Schematic of the measurement setup in the anechoic chamber. The computer, AD/DA converters, and power amplifier are in the adjacent room. In addition to the elements in the schematic, a voltmeter was utilized to measure the voltage over the power amplifier.

installed close to the barometer and the thermometer/hygrometer to allow for external readings of the parameters. A flashlight was used to adjust the light on the displays to ensure readability with the doors to the anechoic chamber closed.

### 3.1.2 Measurement procedure

The measurements were executed by use of the acoustic measurement and analysis program EASERA. A pink noise logarithmic sweep was performed, with EASERA calculating the impulse response from the recorded sound. The microphone was assumed to behave linearly for the sound pressure levels that were generated. Since the chosen measurement quantity was directivity factor or directivity index, it would be necessary to repeat this process for a range of angles. A full rotation was discretized into 91 separate positions, with the first and the last being at normal incidence for the loudspeaker. In other words, measurements were done in 4° steps. Each measurement series then contains 91 calculated impulse responses, which were then used to calculate the directivity factor and the directivity index.

While analyzing data with the purpose of quantifying uncertainties, it is generally beneficial to have multiple sets of data that can be averaged, as averaging reduces the effect of random errors. However, a measurement series generates a large amount of data, and performing the measurement series takes time. For this reason, it was decided to do four measurement series for each measurement setup, to strike a balance between the two considerations – ensuring sufficient amounts of data, while still having enough time to generate and analyze the data.

In order to study the uncertainties involved in the sound scattering process in an anechoic chamber, the effect of certain variable changes was studied. For the measurements performed on the cylinder object, the effect from change of loudspeaker was investigated. Four measurement series were performed for two separate loudspeakers, loudspeaker #1 and loudspeaker #2. In total, eight measurement series were performed on the cylinder object. When measuring using the different loudspeakers, the gain was adjusted to levels that would secure that the volume was high enough to ensure a strong signal arriving at the microphone, while not generating unacceptable levels of distortion. Further details are given in Table A.3 in Appendix A.

For sound scattering measurements done on the box object, there were in total five different measurement setups. For the first two setups, measurements were done with two different loudspeakers, similarly to the cylinder object. Thirdly, measurements were done with the ventilation switched on in the anechoic chamber. For the fourth measurement setup, the box object was removed from the pedestal it was positioned on, and subsequently repositioned. The box was repositioned between each of the four measurement series performed for this setup. Finally, the loudspeaker was removed from its mounting, and repositioned, once again using a laser meter to put it in line with the height of the microphone. In total, twenty measurement series were done for sound scattering on the box object, allowing for the study of four variable changes: change in loudspeaker, ventilation on/off, stationary vs. repositioned receiver, and stationary vs. repositioned source. An overview of all the measurement setups both for the cylinder and the box can be seen in Table 3.1.

Table 3.1: Overview of the sound scattering measurement setups used for the cylinder object and the box object in the anechoic chamber. Four measurement series were performed for each measurement setup.

| **Object** | **Setup** |
|---|---|
| Cylinder | Speaker #1 |
| | Speaker #2 |
| Box | Speaker #1 |
| | Speaker #2 |
| | Ventilation on |
| | Repositioned box |
| | Repositioned speaker |

### 3.1.3 Angle of incidence

While measurements were done in 4° steps for a full rotation around the object, the directivity index was calculated by comparing the recorded sound pressure for normal

incidence with the average[1] for the other angles. For this reason, it is important that the turntable starts at the position which is at normal incidence with regards to the loudspeaker. In order to find this starting point, the turntable was initially sent to +90°, a measurement was then done, before the turntable was sent to -90° for another measurement. The arrival times of the direct sound for those two measurements were compared. The turntable code was then adjusted with an estimated angle of displacement, and the process was repeated until a satisfactory compliance was reached. This was tested to a precision of $\pm$ 0.05°, checking to see if the compliance improved by changing the angle of displacement with 0.1°. Finer increments than this did not seem to make any difference in the compliance between the two arrival times.

An example can be seen in Figure 3.4. Here one can see that the alignment of the peaks in the impulse response for the two angles $\pm$ 90° is best for an angle of displacement of -12.1°, while slightly worse for -12.0° and -12.2°.

For the measurements performed on the cylinder object, the process of finding the angle of displacement was performed before each measurement series. For the box object, however, this was not done as consistently; the process was only done once before the first four measurement series, and once more following said measurements. Overall the discrepancy between these two angles was found to be minor. When comparing angles of displacement before the fifth series and after the sixth series, however, a difference of 0.2° was found. After this, the process was performed before the start of each measurement series.

### 3.1.4 Environmental conditions

In addition to the measurements done, some of the parameters of the conditions in the anechoic chamber were monitored. For the sound scattering measurements done on the cylinder object, the parameters that were monitored were temperature and humidity. This was done by placing a combined thermometer/hygrometer unit near the entrance to the anechoic chamber, and regularly going into the room to check the digital display of the sensor. It would have been preferable to do these readings externally so as not to disturb the conditions of the room, but no such solution was available at this point. There were five readings done for each series; one before measurements were started, then one for each 90° angle until the series was completed. In total for the eight series, there were forty readings of temperature and humidity.

During the sound scattering measurements on the box object, the temperature and humidity were monitored likewise as for the cylinder, but in addition to this, the ambient air pressure was monitored. Further, from the fifth measurement series and onwards, a web camera was installed in the anechoic chamber to allow for readings of the displays without opening the door to the chamber and disrupting the measuring system. A flashlight was used to adjust the light level near the barometer and the thermometer/hygrometer to make the displays readable through the camera. The parameters

[1] The frequency response magnitude squared is averaged for the calculations of the directivity factor.

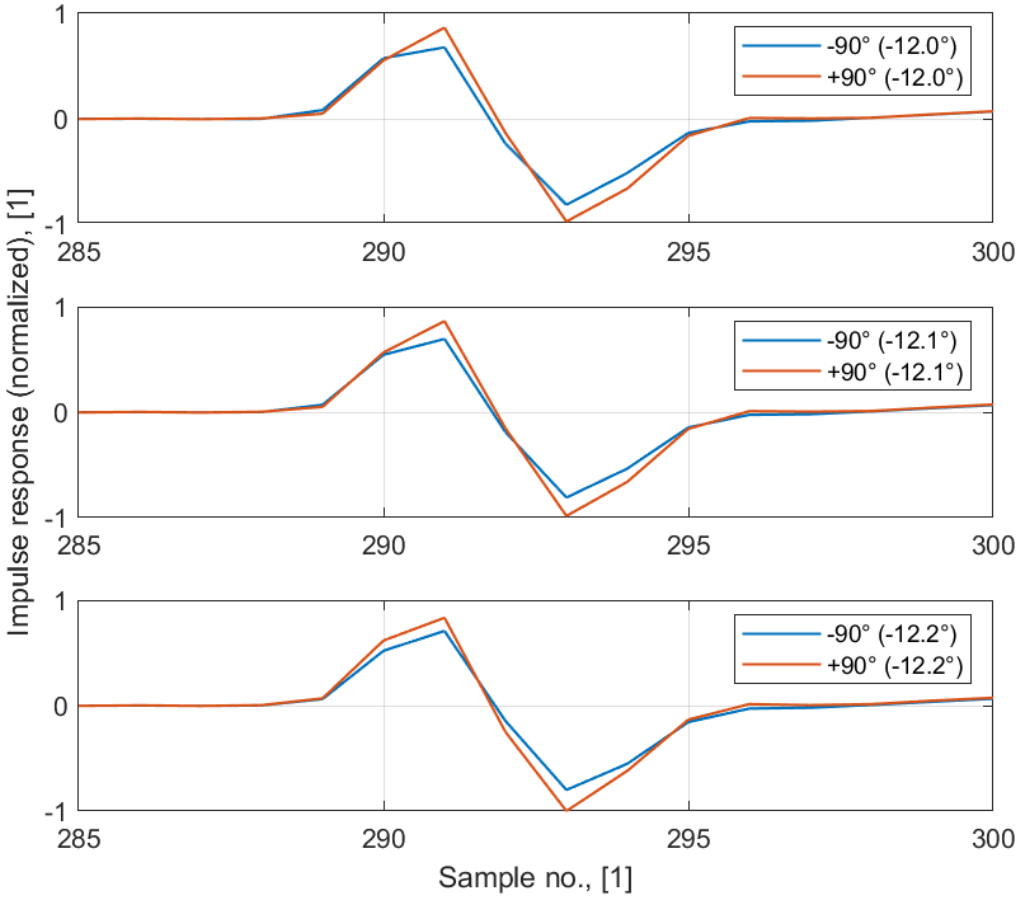


Figure 3.4: Example of the process of finding the displacement angle for normal incidence, where a displacement of -12.1° provides better alignment of the peaks in the impulse response for measurements done at -90° and +90°, as compared to displacement angles of -12.0° and -12.2°.

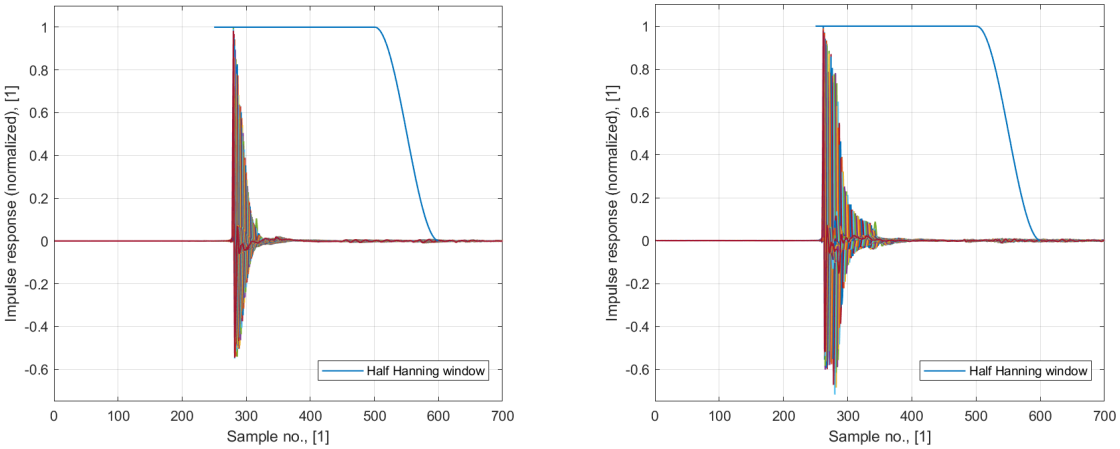


(a) Cylinder object

(b) Box object

Figure 3.5: Impulse responses for the (a) cylinder and (b) box with the half Hanning windowing function used for the discrete Fourier transform shown in blue.

were read for every fifth measurement, adding up to nineteen readings for each measurement series, thus significantly exceeding the five readings for each measurement series performed on the scattering measurements on the cylinder object.

### 3.1.5 Processing of data

Once the impulse responses for each angle were collected, they could be analyzed by use of MATLAB. The frequency response was found from the impulse response by using the discrete Fourier transform. In the process of implementing the Fourier transform, a half Hanning window was utilized to suppress unwanted reflections after the main contribution from the scattering object. The starting point for the window was decided based on the arrival time of the direct sound for the impulse response, and the window had a length of 350 samples. The same window was used for all measurement data. The window is illustrated along with the impulse responses of the cylinder and the box object in Figure 3.5, where the impulse responses are overlaid each other to show their placement with respect to the window.

The frequency spectrum data was then used to calculate the directivity factor, as given in Equation 2.6. The directivity index was calculated from the directivity factor according to Equation 2.7. The calculated directivity index as a function of frequency for each of the four measurement series were averaged for both setups of the cylinder, and all five setups for the box object. The maximum and minimum deviation from the average was also calculated. The difference between this average and its deviation was studied for the previously mentioned comparisons: change in loudspeaker for the cylinder, and change in loudspeaker, ventilation on/off, repositioning of the receiver, and repositioning of the source for the box. These comparisons can be found in Chapter 4.

The directivity index is a function of frequency, and in accordance with what is written in Section 2.1.2, this frequency axis has been converted to a $ka$ number axis by Equation 2.4. As seen in this equation, the $ka$ number is dependent on the frequency $f$ and the velocity of sound, $c$. The velocity of sound was calculated by use of the function "amb2prop" in MATLAB from the "OpenBEM" package [54] (see Section 2.5.1). For this calculation, the monitored variables, namely temperature and humidity, in addition to the air pressure for the box object, were utilized. For the calculations relating to the cylinder, the value 1020 mbar was chosen for the air pressure as it resembled the values observed during the measurements performed on the box. After calculation, the velocity of sound in air for each measurement series was averaged, and the averaged value was used to calculate the $ka$ number axis for the series in question.

## 3.2 Simulations

Simulations of the measurement situation were performed both for the cylinder and the box object. The purpose of simulations were to study the effects of small changes in different variables, which was done by comparing simulations with and without the changes. In the case of the cylinder an analytical solution exists. An expression for the pressure at the surface of an infinitely long, rigid cylinder with an incoming plane wave scattering on it, as given in Equation 2.2, was used as the basis for the simulation. In the case of the box object, no such analytical solution exists, and a MATLAB toolbox built for the purpose of modelling edge diffraction was utilized.

### 3.2.1 Cylinder

A script was written in MATLAB to calculate the pressure at the surface of the cylinder according to Equation 2.2. This equation is valid for an infinitely long, rigid cylinder with plane wave incidence. 50 terms of the sum were used to approximate the solution. The radius of the cylinder as measured on the object under testing was used in the simulation. The previously calculated velocity of sound based on the monitored variables was also utilized. The sound pressure was calculated at several different points around the cylinder, in steps of 4° as in the practical measurements, and was then used to calculate the directivity factor and directivity index according to Equations 2.6 and 2.7 respectively. The simulation was performed with a frequency resolution of 10 Hz, in the range from 50 Hz to 20 000 Hz.

Three different variable changes were studied. Simulations were done with a change in the velocity of sound, the radius of the cylinder, and the offset in angle of normal incidence. For the change in velocity of sound, the reference simulation was done using the average value found during the experimental measurements, while the maximum recorded value recorded was used as a deviation for comparison. For the radius of the cylinder, the measured value was used initially, and the uncertainty was subsequently added to it to give a point of comparison. Lastly, for the angle of normal incidence, tests done during measurements found a change of 0.2° from before and after a completed

measurement series, so the points of calculation around the cylinder were shifted by this factor for the comparative simulation. The results of this study is given in Chapter 4.

### 3.2.2 Box

As there are no analytical solutions available for sound scattering on a box object, the simulations of the measurement system was performed by use of the MATLAB toolbox "EDtoolbox" created by Peter Svensson [32]. More details about this toolbox can be found in Section 2.1.3. The parameters from the measurement setup in the anechoic chamber were implemented; the average values for the dimensions of the box as given in Table A.2 in Appendix A, along with the average distance between the microphone and the two different loudspeakers, and the average velocity of sound in air as calculated from the monitored environmental conditions (temperature, humidity, pressure). For other conditions such as the density of air, default values from the toolbox were used [32].

The simulations were done with a frequency resolution of 10 Hz, similar to the simulations for the cylinder. A range of 100 Hz to 20 000 Hz was used. The edge diffraction based toolbox discretizes the edges of the simulated object, and the number of points for the longest edge can be provided as input from the user through the parameter "ngauss". The calculation time depends exponentially on the value of this parameter. While the author of the toolbox has recommended using a minimum of three points per wavelength of the highest frequency to be simulated, such a high resolution would lead to a prohibitively long runtime for the simulation. Thus, tests were run to see what resolution would be necessary in order to limit the deviation of the directivity index at selected frequencies within a chosen precision boundary, from the previously mentioned recommended discretization. The results of these tests can be seen in Figure 3.6.

In Figure 3.6, (a) illustrates the directivity index calculated when using different values for ngauss at a frequency of 10 kHz while (b) shows the same for 20 kHz. In order to follow the recommendation of the toolbox author of three points per wavelength for the highest frequency, an ngauss value of 68 would be required. For this reason, the directivity index calculated with this number of discrete edge points, $DI_{68}$, is used as a reference value. A deviation from this corresponding to 1/1000 of the value, in decibels equal to $\pm\,0.0043$ dB, is illustrated with a dashed line for both frequencies. As can be seen in Figure 3.6(a), the simulated directivity index converges within the $\pm\,0.0043$ dB lines of deviation at a point between the ngauss values of 30 and 35. However, looking at Figure 3.6(b), the convergence for a frequency of 20 kHz does not occur until a later point, first properly crossing the dashed lines for an ngauss value of 47. Due to this result, the longest side of the box was divided into 47 points rather than the advised 68 points, to reduce the calculation time.

The same variable changes that were studied for the cylinder were also studied for the box, specifically the velocity of sound, the dimensions of the box, and the offset angle for normal incidence. The magnitude of these changes were consistent with the obser-

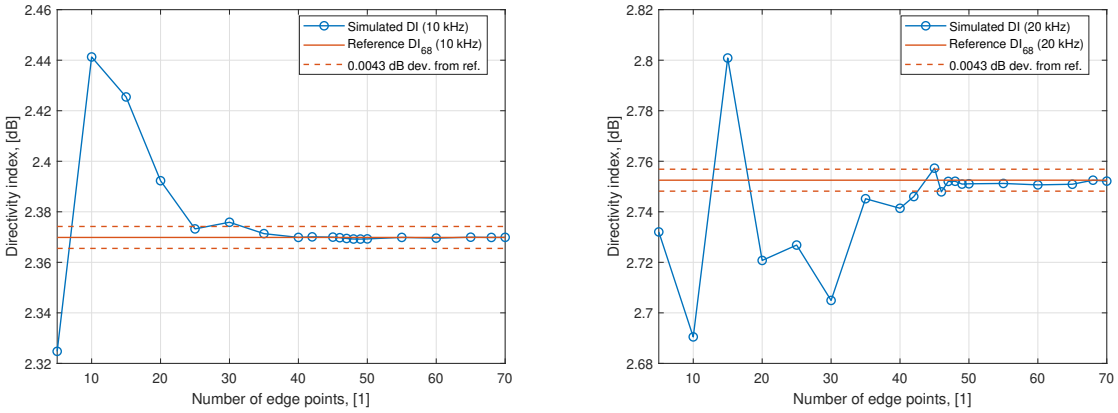


(a) 10 kHz (b) 20 kHz

Figure 3.6: Simulated directivity index for the box by use of different values for the number of edge points ("ngauss"), at the frequency of (a) 10 kHz and (b) 20 kHz. Includes the reference value for ngauss = 68, with a deviation of 0.0043 dB in dashed lines.

vations from the experimental measurements for the box. For the velocity of sound, the reference simulation utilizing the average value was compared with the minimum value recorded during measurements, as this had a larger deviation from the average than the maximum value. This is different from the cylinder simulation, where the maximum value was used for comparison. For the box dimensions, the original simulation was done with the averaged measured values, while the comparison simulation was run with the measurement uncertainty added, giving a maximum value for these dimensions. For the angle of incidence, a magnitude of 0.2° change from testing before and after a completed measurement series was found for the box as well. Hence, the comparison simulation used this shift in the placement points for the simulated receivers around the box. Similarly to the cylinder, the results of these comparisons are given in Chapter 4.

# Chapter 4

# Results and Discussion

In this chapter the results found during the work of this thesis will be presented and discussed. First are the results relating to the experimental proceedings, both for the cylinder and the box, followed by those gained from simulations. Lastly is a section finalizing the discussion of the results.

## 4.1 Measurements

Measurements were performed as outlined in Chapter 3. Following is a section on the results collected from monitoring the environmental conditions in the anechoic chamber, and a section about the post-processing of the measured data where the calculated directivity indices found for the cylinder and the box are presented.

### 4.1.1 Environmental conditions

During the sound scattering measurements that were performed on the cylinder object and the box object, the value of certain environmental conditions were recorded. For the duration of the measurements done on the cylinder, the temperature and the humidity were both recorded, while during the measurements done on the box, the air pressure was monitored as well. The global variations of these variables are shown in Figure 4.1 and Figure 4.2, giving the average value for each measurement series performed, as well as indicating the point of the average value for each measurement setup.

For the interested reader, a closer look a the local variations that go into these averages can be seen for an arbitrarily chosen measurement setup in Figures B.1 and B.2 in Appendix B, where the first figure shows the local variations for both measurement setups that were utilized for the cylinder object. In these figures, it is notable that the monitored variables seem to change in a somewhat linear fashion, and making measurements over a short amount of time limits the range of these variables from start to finish.

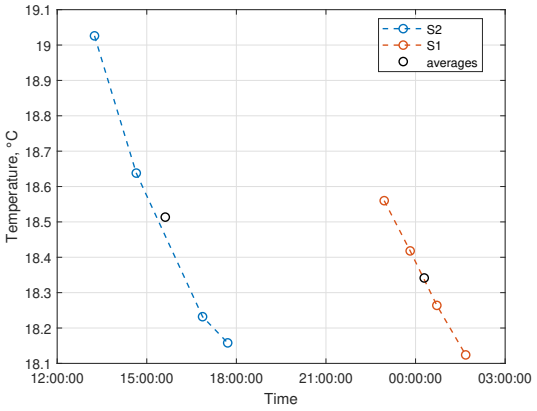


(a) Temperature

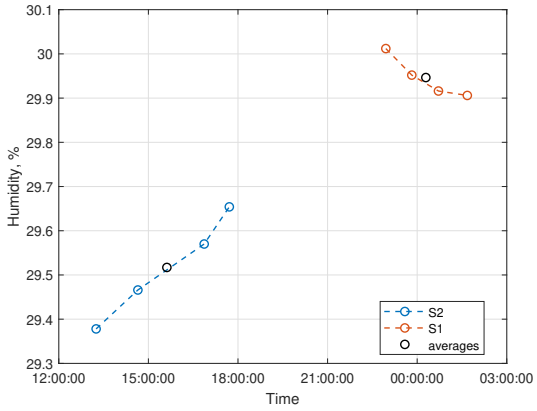


(b) Humidity

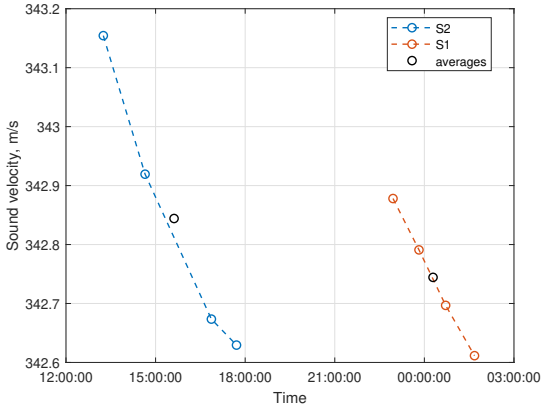


(c) Velocity of sound

Figure 4.1: Global trends of environmental conditions that were monitored during sound scattering measurements performed on the cylinder object; (a) temperature, (b) humidity, and (c) calculated velocity of sound from the monitored variables. The labels indicate which measurement series the conditions have been monitored during, where "S2" in blue is loudspeaker #2 while "S1" in red is loudspeaker #1.

The velocity of sound in air was calculated as indicated in Section 3.1, using the monitored values as input. For the calculations related to the cylinder, the air pressure was not monitored, and the value of 1020 mbar (resembling the values seen during the measurements performed on the box) has been used as a constant air pressure level. While an assumption of constant air pressure with this value is unlikely to accurately portray what would have been found if it had been monitored, the measurements on the cylinder were done in a short span of time, meaning the air pressure is unlikely to have varied much. The weather was also stable during this time, and the monitored values during the box measurements indicate that sudden weather changes are the largest source of air pressure changes of noticeable extent, as will be elaborated shortly. The calculated velocity of sound in air is included in Figure 4.1 and Figure 4.2.

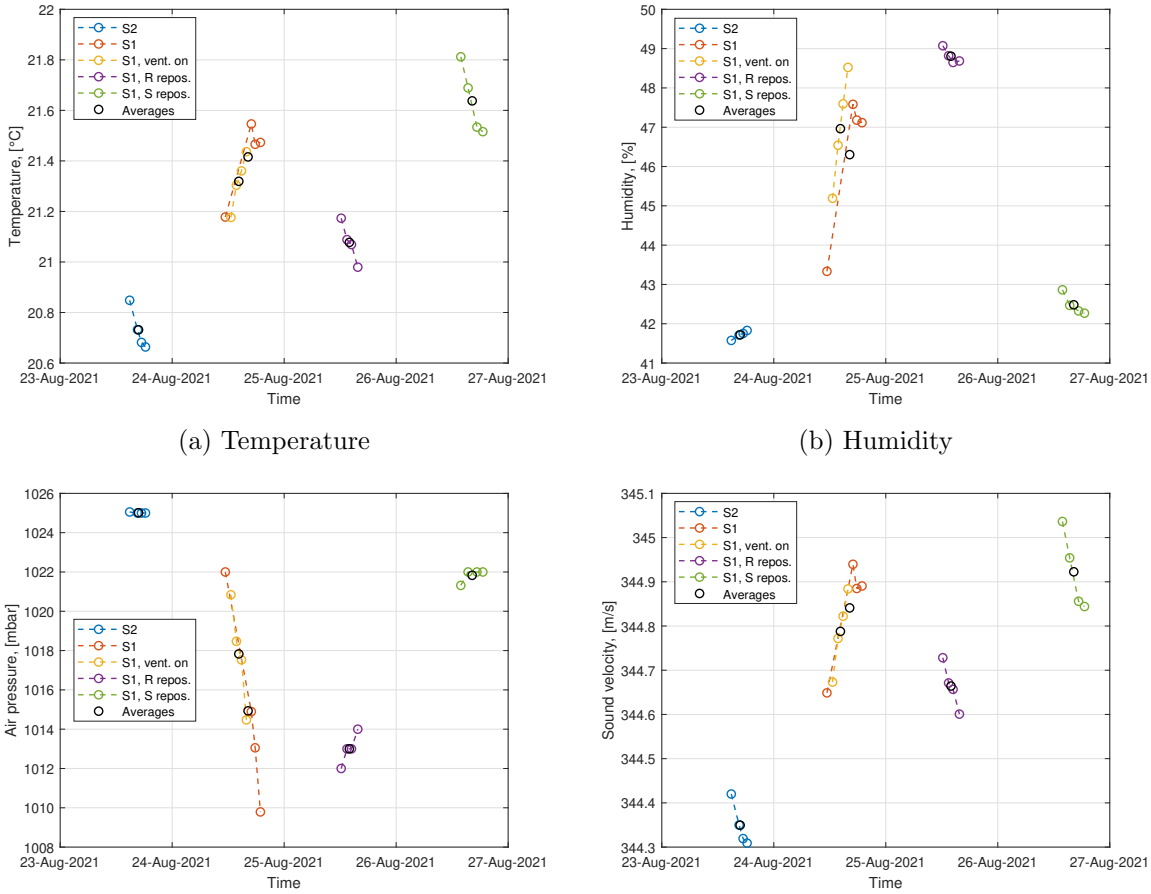


(a) Temperature

(b) Humidity

(c) Ambient air pressure

(d) Velocity of sound

Figure 4.2: Global trends of environmental conditions that were monitored during sound scattering measurements performed on the box object; (a) temperature, (b) humidity, (c) ambient air pressure, and (d) calculated velocity of sound from the monitored variables. The labels indicate which measurement setup the environmental conditions have been monitored during, with "S2" in blue being the setup using loudspeaker #2, "S1" in red is using loudspeaker #1, the curve in yellow is with the ventilation system on, the curve in purple is with the microphone and scattering object being repositioned between each measurement series, and the curve in green is for the loudspeaker being repositioned between each measurement series.

In Figure 4.1, one can see the average temperature for each of the eight measurement series in (a) with the time stamp on the x-axis, while (b) shows the humidity and (c) shows the corresponding calculated velocity of sound. As can be seen upon comparison of these three figures, the velocity of sound seems largely dependent on the temperature, as the curves in (a) and (c) are nearly identical. The variation in temperature ranges approximately 1°C from slightly higher than 18.1 °C to nearly 19.1 °C, while the humidity ranges approximately 0.6%. Thus, the temperature has the largest impact on the calculated velocity of sound, which ranges from slightly higher than 342.6 m/s to almost 343.2 m/s.

Studying Figure 4.2 which shows the environmental conditions as monitored during the measurements on the box object, there is a similar occurrence of the temperature curve in (a) being very similar to the curves for velocity of sound in (d). Here one can also see how the ambient air pressure changed during the measurements, extending from 1009 mbar to 1025 mbar. The changes in the air pressure coincide with weather changes between the days when measurements were performed and the environmental conditions were monitored. Looking at the temperature and humidity variations in Figure 4.2, this weather change seems to have affected all environmental conditions.

There appears to be an inverse proportionality in the behavior of the humidity in (b) and the ambient air pressure in (c), where the trends resemble a mirror image of each other. It is notable that the measurements performed on the box have been done over a much larger time span compared to the cylinder, ranging several days rather than several hours. This also results in a larger range for the monitored values, where, although the temperature only varies by approximately 1.2°C from slightly higher than 20.6 °C to a little over 21.8 °C, humidity spans close to 8% from about 41.5% to over 49%.

In conclusion, however, similarly to the cylinder, the temperature appears to be the main influencing factor for the calculated velocity of sound during measurements on the box as well. The resulting range for the velocity of sound is 344.3 m/s to nearly 345.1 m/s. While the ranges are only slightly increased, the temperature itself is a few degrees higher for the measurements done on the box, which could be an explanation for why the actual values of the velocity of sound are a bit higher. This temperature difference in the anechoic chamber is likely explained by the measurements on the cylinder having been done in April while the measurements on the box were done in August.

### 4.1.2 Processing of data: Cylinder

#### Directivity factor

From the measurements in different points of a full rotation of the cylinder on the turntable, the directivity factor was calculated according to Equation 2.6. In addition, measurements of the ambient noise were performed. These were done by doing the same measurement in EASERA, albeit with the loudspeaker disconnected, resulting

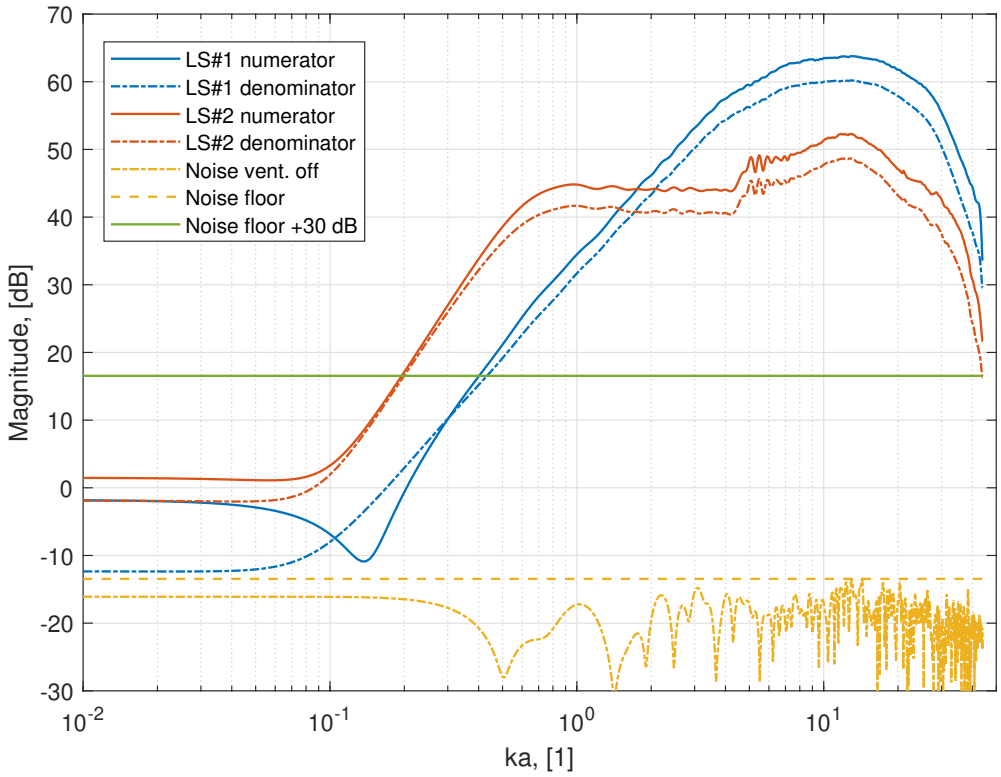


Figure 4.3: Calculated directivity factor, estimated noise floor, and cutoff level for measurements performed on the cylinder, where the directivity factor is plotted with the numerator and the denominator separately.

in the calculated impulse response from the program. The difference in decibels between the noise and the directivity factor can be noted as the signal-to-noise ratio, in accordance with Section 2.3.2. The directivity factor from one of the measured series using each of the loudspeakers, with the numerator and denominator of Equation 2.6 shown separately, is illustrated along with the noise in Figure 4.3. The spectral shape of the noise seems quite flat, and the highest peak in the interesting frequency range has been used to represent the noise floor, with a line being drawn in the figure to indicate this. If choosing 30 decibels as an appropriate signal-to-noise ratio for deeming measured response as reliable, then another line can be drawn 30 decibels above the estimated noise floor to indicate this. The frequency where the directivity factor for the microphone, measured with each of the two different loudspeakers, cross this 30 dB above noise floor line then gives an estimated cutoff value for when the calculated directivity factor, and hence directivity index, contains reliable information. The point where these lines intersect was recorded, and is given further below in Table 4.1.

### Cutoff value

As shown in Figure 4.3 the cutoff value is higher for loudspeaker #1 than for loudspeaker #2. In other words, for these measurements loudspeaker #2 would have a larger range for lower frequencies. With that said, one can observe that there is a region with oscillations around $ka$ values 4.5 to 8 for loudspeaker #2, which does not occur for loudspeaker #1. These oscillations might be caused by resonances in the membrane of the loudspeaker, or within the pipe that the loudspeaker element is mounted within since the mounting setups of the loudspeakers differed (seen in Figures 3.1 and 3.2). Due to these findings, loudspeaker #1 may be more appropriate if one wants to study phenomena at higher frequencies, while loudspeaker #2 could be a better choice if the frequencies of interest are in the lower range.

The following figures for experimental data include only the values of the $ka$ number which are within the area of reliable information. This means that for figures where measurements from both speakers are included, the limitations of loudspeaker #1, which has a higher cutoff value at low frequencies, are applied. As the line for the denominator of loudspeaker #2 narrowly crosses the cutoff line, there is an upper cutoff for this loudspeaker approaching 24 kHz. The exact value can be found in Table 4.1, given in the next section.

### The $ka$ value problem

There are four measurement series for each setup, and the directivity factor found for each series is averaged according to Equation 2.14. However, since the environmental conditions vary slightly, the different measurement series also have different $ka$ values for each discrete point, because $k = 2\pi f/c$, and $c$ changes from one series to the next. This distinction can be seen in Figure 4.4, where the same frequency value has been marked on each curve. In 4.4(a) the same value of the velocity of sound, $c$, has been used for all curves, resulting in the same $ka$ values for each individual point. In 4.4(b) individual values of $c$ have been utilized for each series. As one can see, the difference between the curves is reduced, which is explained by the absence of a horizontal shift.

In order to find the maximum deviation in positive and negative direction from the average directivity factor, the difference is calculated not for the same frequency values, both for the frequency values which give $ka$ values that are closest in horizontal distance to the average point. From what is seen in Figure 4.4(b), this entails comparing points that lie as close to each other as possible on a vertical line through each point of the average value. The index of these points are found, and this so-called best index point on each curve is used when finding the maximum deviation from the mean. One should keep in mind, however, that this does not ensure an entirely precise value for the deviation from the mean as the discrete points to do not line up perfectly, but it does reduce some of the error in estimation that would be present otherwise. Having found the values for the mean directivity index and its deviations, the directivity index is calculated according to Equation 2.7. The average directivity index with its upper and lower maximum deviation is shown in Figure 4.5.

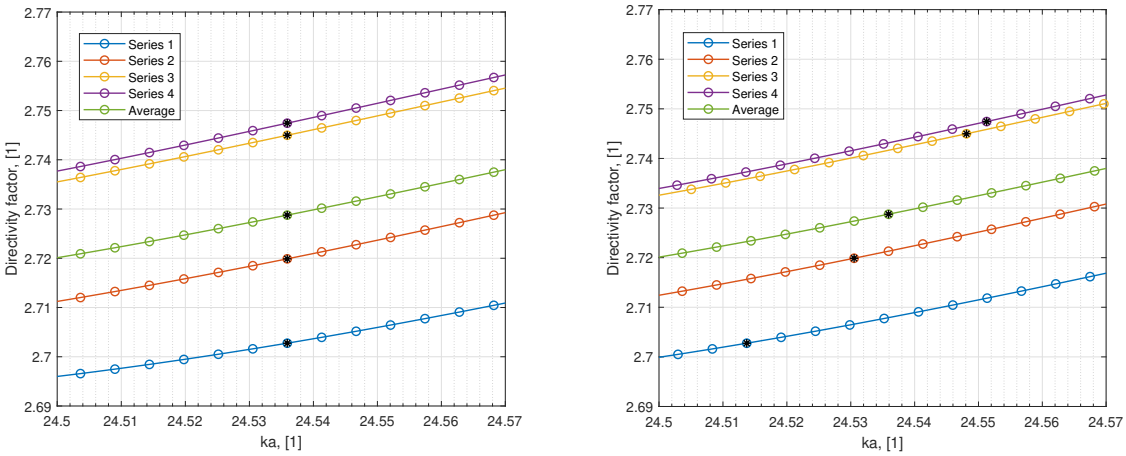


(a) Same value of $c$ used for all series.

(b) Individual values of $c$ used for all series.

Figure 4.4: Measured and average directivity factor for the cylinder, shown with (a) the same $ka$ values for every series, and (b) individual $ka$ values for each series and average $ka$ values for the average directivity factor. The same frequency value is marked in black on all curves in both subfigures.

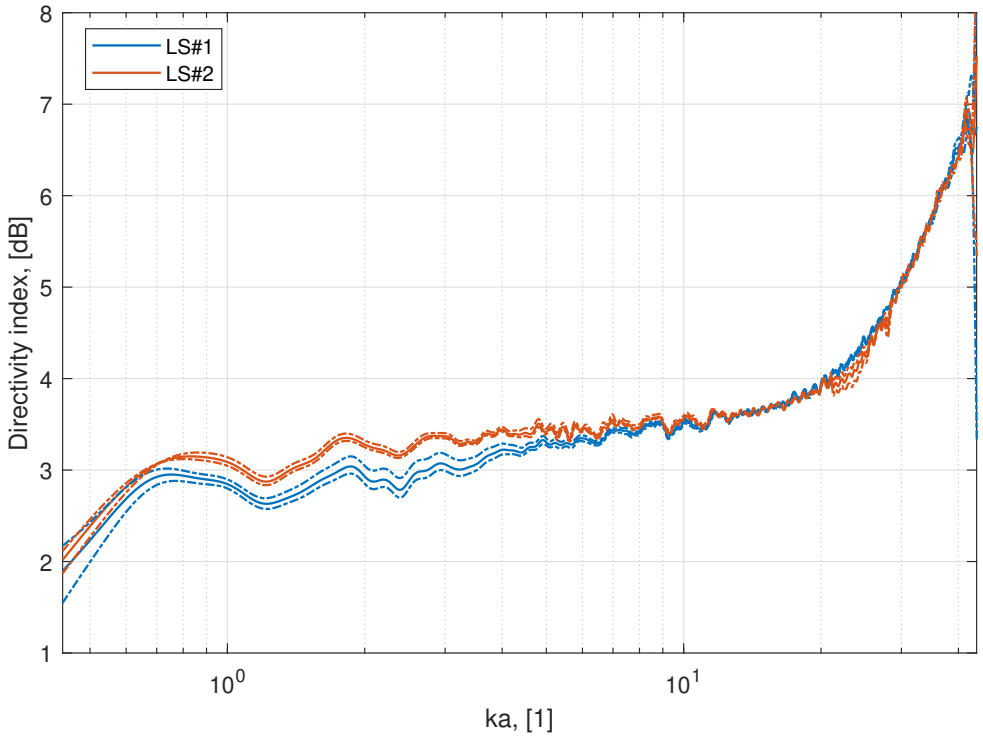


Figure 4.5: Averaged measured directivity index for the cylinder object, with the dotted line indicating the deviation from the mean for the four measurement series incorporated in the mean, with loudspeaker #1 in blue and loudspeaker #2 in red.

### Directivity index

As seen in Figure 4.5, the directivity index for both loudspeakers when measured on the cylinder stays between 2.5 and 3.5 for most of the frequency range up to a $ka$ number of about 10, while after this increasing for increasing frequency values up to a value of 7-8. A rapid change in the directivity index can be observed at the upper bounds of the figure, which could indicate that a lower cutoff value than what was estimated with Figure 4.3 should have been used.

Another observation from Figure 4.5 is that the largest discrepancy between the two speakers is in the lower frequency range, and that they follow each other closely for $ka$ numbers above approximately 7, with the exception of an area of oscillations in the results generated by loudspeaker #2 between $ka$ values 20 and 30. These oscillations do not coincide with those seen in Figure 4.3, which occur in the region of $ka$ number 4.5 to 8. However, this secondary oscillation region seen in Figure 4.5 may stem from a different resonance frequency occurring in the loudspeaker pipe or membrane.

### Difference in directivity index

A closer look at the difference between the averages of the two loudspeakers can be seen in Figure 4.6, with the difference between the two means shown as a solid line and the maximum difference between the deviation from mean given as a dotted line. The difference is evidently greatest for the lower frequency range, while gradually decreasing and dropping below zero for higher frequencies, before a subsequent increase. The difference has been calculated by subtracting the value found using loudspeaker #1 from that found using loudspeaker #2. This means that for lower frequencies, the first loudspeaker gives lower values for the directivity index than the second, while the opposite is true for a subset of the higher frequency values. The difference between the two loudspeakers, however, remains less than 0.6 dB when discounting the very highest frequencies plotted in the figure. As stated in the previous paragraph, the sudden increase seen for the highest frequencies may be an indication of the realistic upper cutoff value being lower than what was estimated.

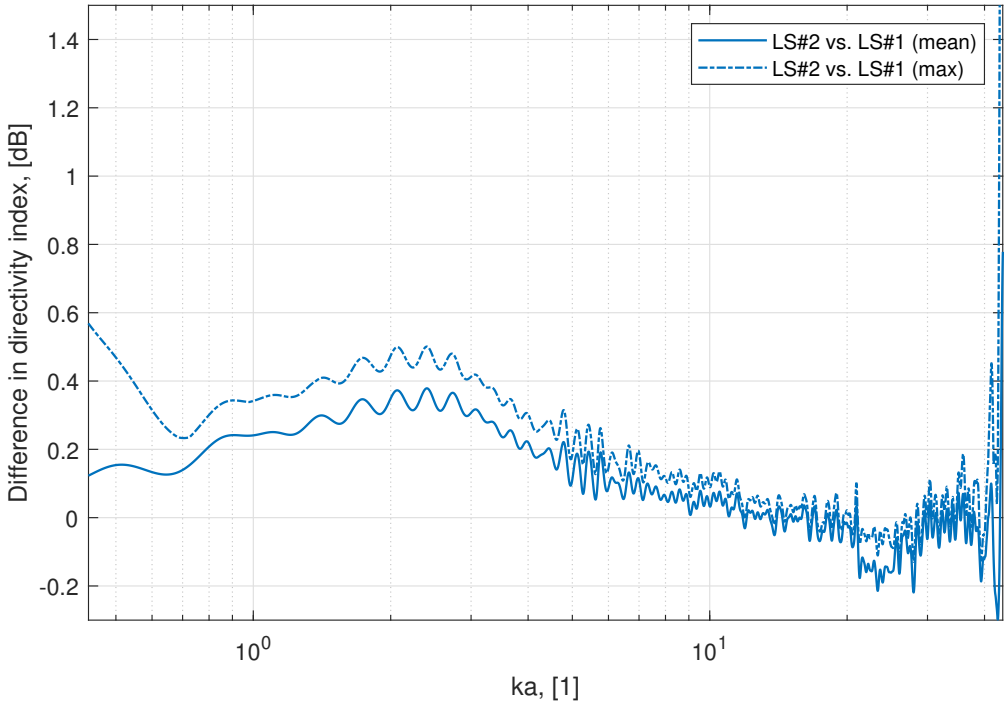


Figure 4.6: Difference in averaged measured directivity index for the cylinder object, using two different loudspeakers. Includes the maximum difference between the deviation from the mean. The difference is calculated by subtracting the directivity index given by loudspeaker #1 from that given by loudspeaker #2.

### 4.1.3 Processing of data: Box

#### Directivity factor and cutoff value

As for the cylinder, the measurements for the box were used to calculate the directivity factor. The numerator and the denominator of this calculation, along with the measured noise in the anechoic chamber, is presented in Figure 4.7. In this figure there are two measured values for noise; one is with the ventilation off, and one is with the ventilation on. For these noise measurements the level is higher at the lowest frequencies as compared to the rest, but as found previously the lowermost frequencies fall outside the domain of reliable information. Due to this, the maximum value of the entire curve was used to find a maximum possible level for the noise floor, giving an indication of the possible cutoff frequency. In this estimation, however, the lower frequency ranges of the noise, which formed the basis of the noise floor, were outside the range of reliable information. A new estimation was then done, which neglected the values below $kl$ number equal to approximately 0.6. This distinction was done based on the appearance of the noise being constant rather than seeming to contain much information. The new noise floor was then used to find a new cutoff, where the basis for the noise floor was within the area of reliable information. The cutoff values found through this figure, as well as by use of Figure 4.3 for the cylinder, can be found in Table 4.1.

Table 4.1: Cutoff values for measurements done with the cylinder and the box, based on values having to be more than 30 dB higher than the estimated noise floor. Data collected from Figures 4.3 and 4.7.

| **Object** | **Loud-speaker** | **Lower cutoff [ka/kl]** | **Lower cutoff [Hz]** | **Upper cutoff [ka/kl]** | **Upper cutoff [kHz]** |
|---|---|---|---|---|---|
| Cylinder | Speaker #1 | 0.435 | 237 | - | - |
| | Speaker #2 | 0.204 | 111 | 43.9 | 23.9 |
| Box | Speaker #1 | 1.70 | 267 | - | - |
| | Speaker #2 | 0.748 | 117 | 139 | 21.9 |

In Figure 4.7 one can see the same trend as in Figure 4.3: the lower cutoff value for loudspeaker #1 is slightly higher than that of loudspeaker #2. Here one can also see that the directivity factor as found using loudspeaker #2 more clearly crosses the line for 30 dB above the noise floor; as stated in Table 4.1, the upper cutoff value is also lower than that found for the measurements on the cylinder when comparing the frequency values in hertz.

The directivity factor curves in Figure 4.7 contain some large-scale oscillations. These are distinct for the numerator but not for the denominator, which in other words means that when averaging over all the angles of measurement, these oscillations cancel out. Interestingly, the oscillations in the numerator appear very similar between the two

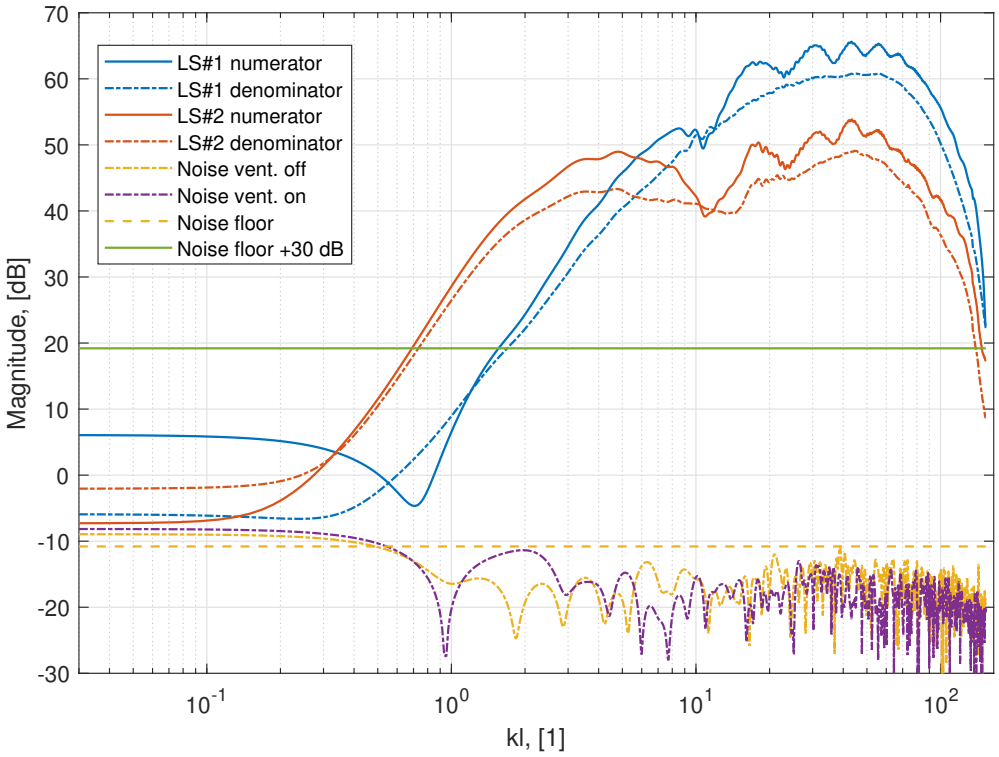


Figure 4.7: Calculated directivity factor, estimated noise floor, and cutoff level for measurements performed on the box, where the directivity factor is plotted with the numerator and the denominator separately. The noise has two separate measurements, one with the ventilation off and one with the ventilation on.

loudspeakers; they have troughs and peaks at similar $kl$ numbers, which could indicate that this is a phenomenon caused by either the geometry of the box object, or possibly the post-processing of the data. With the oscillations not appearing in the denominator, the geometry is likely responsible for this behavior, without speculating further into the mechanics behind it. As will become apparent in Section 4.2.2, the same large-scale oscillations will be seen for simulations of the box (Figure 4.13), further strengthening the theory of this being caused by the geometry of the object.

One can also notice a hint of the same oscillations as were seen from loudspeaker #2 in Figure 4.3, now for $kl$ values of around 17 to 25. They are not as distinct as for the cylinder, but are evident from the dashed red line for the denominator of the directivity factor given by loudspeaker #2. There are also oscillations present from loudspeaker #1 which have not been observed for the cylinder around $kl$ values of approximately 9 to 13, around the first trough for the previously mentioned large-scale oscillations. While the large-scale oscillations do not appear in the denominator, the ripple for these $kl$ values can be observed, and could indicate the presence of a resonance frequency within the box object itself.

### Directivity index

Five different measurement setups were used for the measurements on the box, as given in Table 3.1. With each setup containing four measurement series repeating the same measurements, the directivity factor that was found is averaged in the same way as for the cylinder measurements, and recorded along with the deviation from the mean. From the directivity factor, the directivity index is calculated according to Equation 2.7. In order to be able to compare with Figure 4.5 for the cylinder, the averaged directivity index for the setups using loudspeaker #1 and loudspeaker #2 are illustrated in Figure 4.8. The directivity index for the other setups are not illustrated here but showed similar behavior.

Noticeably, there are differences between the directivity index for the box in Figure 4.8 and that of the cylinder in Figure 4.5. The curves for the box show large-scale oscillations that were not seen previously, which can be recognized from the numerator curves in Figure 4.7. The first three peaks occur at $kl$ values of approximately 6, 16, and 30, with the first troughs at $kl$ values of about 11, 23, and 37. As noted previously, these large-scale oscillations are likely due to the geometry of the box. It disappears during the averaging of the denominator in Equation 2.6, but remains in the numerator causing the same oscillation in the directivity index.

The two averages mostly inhibit similar values; up until a $kl$ number of approximately 8, loudspeaker #1 gives a slightly lower directivity index, but following this region the difference becomes less distinguishable. There is notably an area around $kl$ value 70 to 85 where loudspeaker #1 gives a slightly higher directivity index compared to loudspeaker #2. This does not coincide with the resonance frequencies suggested previously in relation with Figure 4.7, which were located in regions with $kl$ values of 9 to 13 and 17 to 25. The trend in directivity index observed at these higher $kl$ values does not

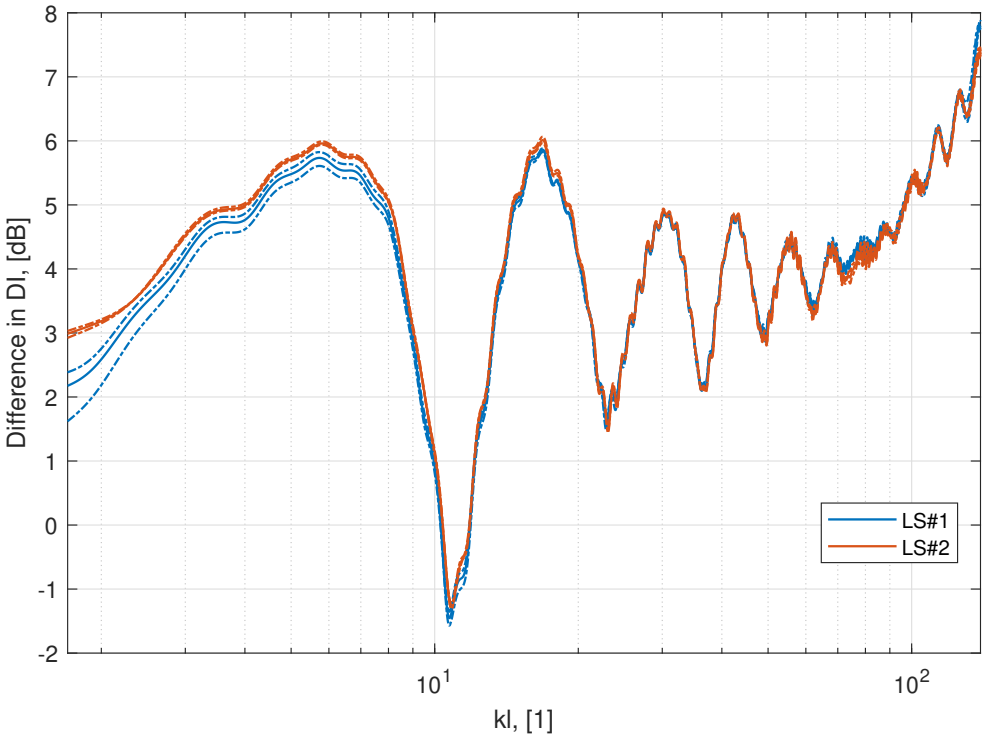


Figure 4.8: Averaged measured directivity index for the box object, where the dotted line indicates the deviation from the mean. Results from loudspeaker #1 is given in blue while those from loudspeaker #2 is in red.

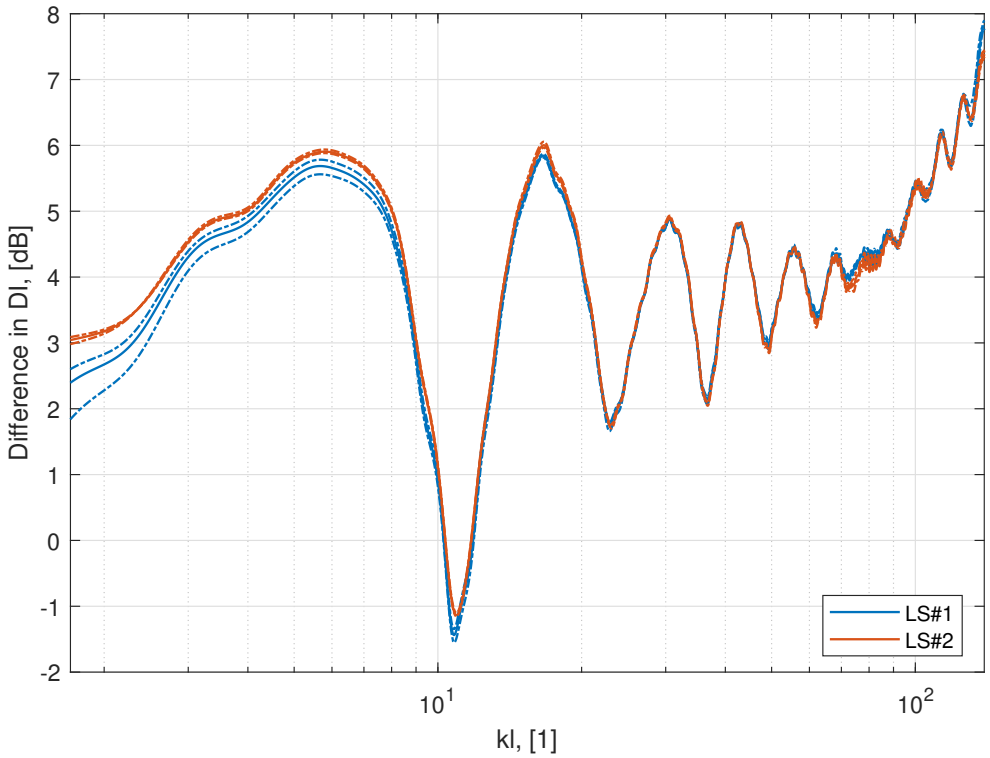


Figure 4.9: Averaged measured directivity index for the box object when using a time window spanning 300 samples instead of 350 samples, with the same starting time.

have an immediately obvious explanation.

In addition to the large-scale oscillations, there are numerous small-scale oscillations following the curve. This was seen for the cylinder as well, but appears to be more pronounced for the box. A possible cause is unwanted early reflections being included as input when the discrete Fourier transformation is performed. For this reason, the post-processing was repeated using a slightly shorter time window, with a length of 300 samples instead of 350. The resulting directivity index can be seen in Figure 4.9.

As can be seen in Figure 4.9, the small-scale oscillations have been greatly reduced. In other words, these were most likely caused by unwanted reflections being included in the windowed data. With that said, the other trends in the figure remain the same as in Figure 4.8, and the discussion of these trends still stands. Further processing of these results, however, will be based on that generated by use of a shortened time window.

### Difference in directivity index

Due to the similar shapes of the directivity index curves, more information can be gained from studying the difference between the means, in addition to the difference between the deviations. For each comparison of measurement setups, a subplot is generated to illustrate these values. This is shown in Figure 4.10.

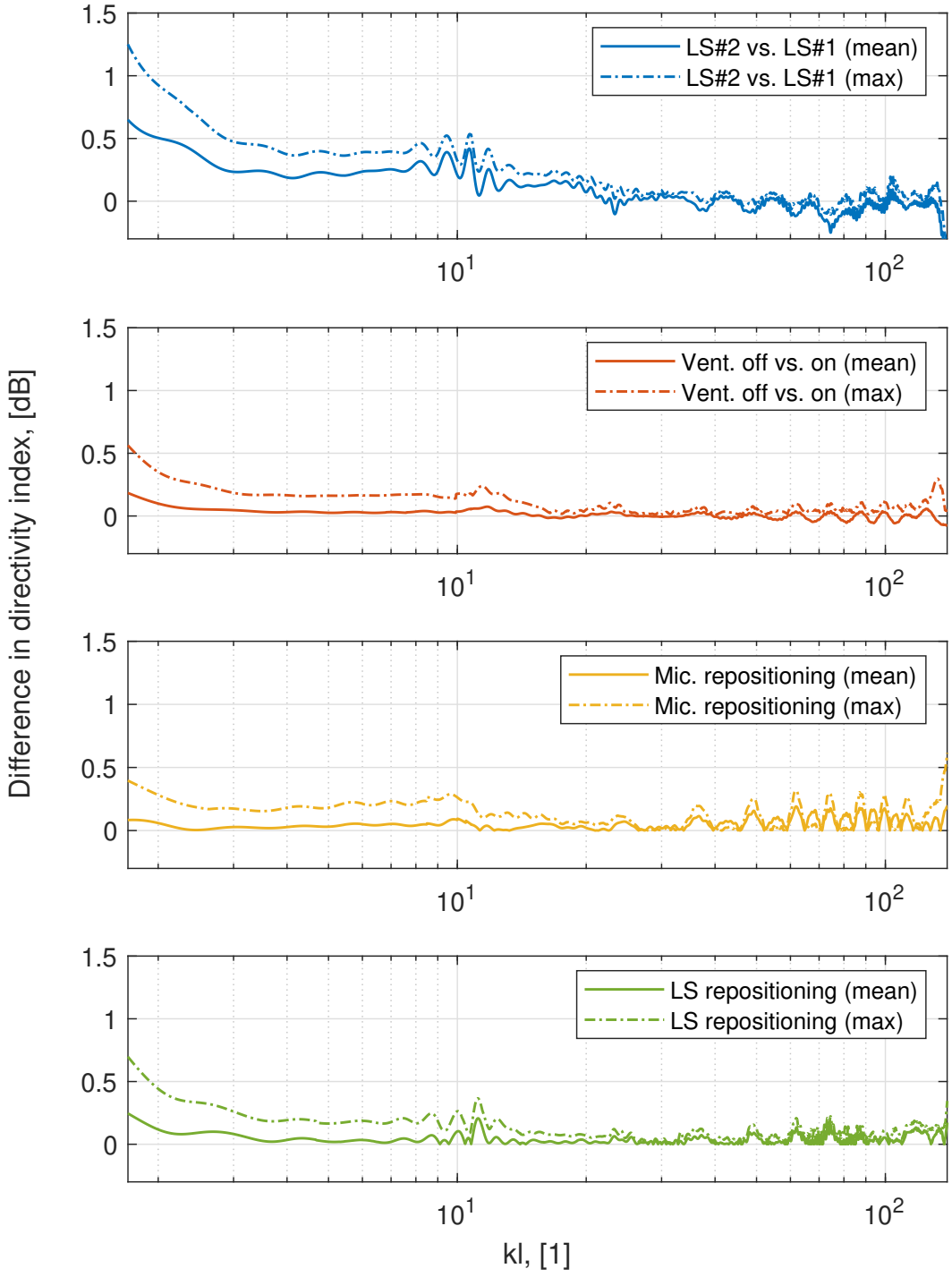


Figure 4.10: Difference in average measured directivity index on the box object, for (a) two different loudspeakers, (b) ventilation on and off, (c) repositioning the microphone, and (d) repositioning the loudspeaker. The last two are shown in absolute values.

The first part of Figure 4.10 shows the difference in directivity index given by the two different loudspeakers that have been used. This is equivalent to Figure 4.6 for the cylinder object. The difference between the two loudspeakers is calculated by subtracting the measurements using loudspeaker #1 from those using loudspeaker #2, as was done for the measurements on the cylinder. From Figure 4.10 then, loudspeaker #2 gives a larger directivity index for the lower frequencies, as noted for Figure 4.8, until some oscillations around $kl$ value 10, when the difference decreases a bit. There is another set of oscillations around $kl$ value 20, and here the difference oscillates around zero. The difference never exceeds 1.5 decibels, being less than $\pm$ 0.5 dB after $kl$ value approximately 3, and under half of that again after $kl$ number circa 13. The difference between the maximum deviations from mean are slightly higher for low frequencies, but have similar magnitude for values above $kl$ number 30. Comparing the figure as a whole to that for the cylinder (Figure 4.6) the magnitudes of the difference are within the same range if neglecting the values below $kl$ number 3 for the box.

The second part of Figure 4.10 shows a comparison between having the ventilation system in the anechoic chamber turned off or on. The values found with ventilation on are subtracted from those with ventilation off to give this difference. The third part of the figure shows the difference between the microphone being repositioned between each measurement series and the microphone being left stationary, while the fourth part of the figure shows a comparison between repositioning the loudspeaker between each measurement series and leaving it stationary.

On a whole, the three comparisons show the same oscillation around $kl$ number 10, with that of the ventilation on/off comparison additionally showing the oscillation after $kl$ number 20 as for the loudspeaker comparison. All three differences remain less than 0.5 dB aside from the lowermost frequencies, and they all have an increasing degree of oscillation for the higher frequencies. From what is found in this figure, the four factors that have been studied show similar magnitudes in how much their alterations affect the directivity index.

## 4.2 Simulations

Simulations were performed as described in Chapter 3. In the following section the simulated results for the cylinder object based on the analytical solution, including the simulated directivity index and the corresponding change in directivity index from a change in selected variables are presented. The simulated variable changes were deviation in velocity of sound, deviation in the displacement angle for the normal incidence, and deviation in the radius of the cylinder object. This is followed by a section about the simulated results for the box object based on the ESIE numerical solution, which also includes the directivity index, and the change in directivity index from equivalent variable changes as for the cylinder.

### 4.2.1 Cylinder

#### Directivity index

Based on the monitored environmental conditions, the simulation by use of the analytical solution for an ideal infinitely long cylinder were performed, using the average value of the velocity of sound for all measurement series done on the cylinder object. As for the calculations presented in Figure 4.1 in Section 4.1.1, the value of the air pressure was set to 1020 mbar. Using a range of 50 Hz to 20 kHz, with a resolution of 10 Hz, the resulting simulated directivity index for the cylinder object can be seen in Figure 4.11. Three other curves are included in this figure, which will be elaborated upon shortly.

As can be seen in Figure 4.11, the directivity index increases rapidly from the lowest $ka$ values until it starts approaching a value of 3 dB, around $ka = 0.8$. After this the directivity index oscillates slightly while overall trending slightly upwards, until stabilizing for oscillations around a directivity index of about 3.1 dB. This stabilization happens around $ka$ value 5-6. At this point the oscillations become decrease in amplitude.

#### Difference in directivity index

The simulations are intended to allow the estimation of how certain variable changes might affect the directivity index. For this purpose, the simulation was repeated with a slight change in the velocity of sound, based on the maximum deviation seen in the sound velocity from the measurements, for a slight displacement in the angle of normal incidence according to the observations from the process of finding the necessary displacement for the turntable for normal incidence, and for a deviation in the radius of the cylinder according to the uncertainty that was found when measuring the dimensions of the constructed cylinder object. Separate simulations have been run for these changes, and are all illustrated in Figure 4.11.

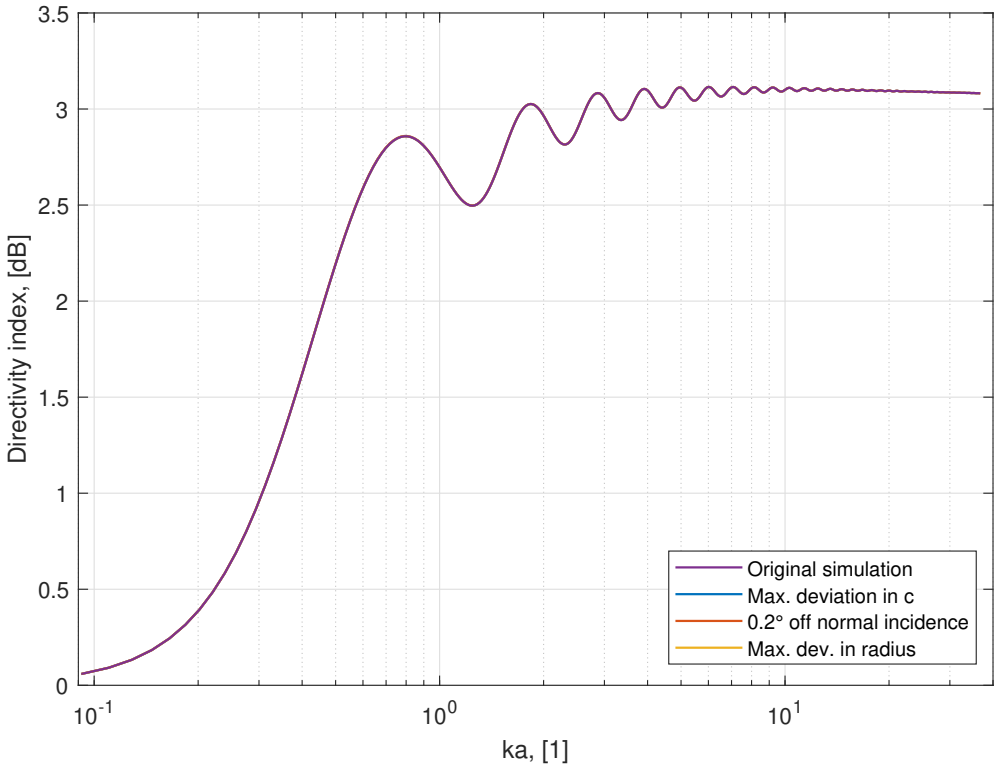


Figure 4.11: Simulated directivity index as a function of $ka$ number for the cylinder object, with four different sets of input data including a reference and minor differences in selected variables: velocity of sound, angle of displacement for normal incidence, and radius of the cylinder object. The simulation is done by use of the analytical solution for an ideal, infinitely long cylinder.

With that said, the resulting directivity indices were so similar in value that the curves are not distinguishable from each other in Figure 4.11. For this reason, the difference between the three variable changes as compared to the original measurement, which here functions as a reference simulation, are studied more closely in Figure 4.12.

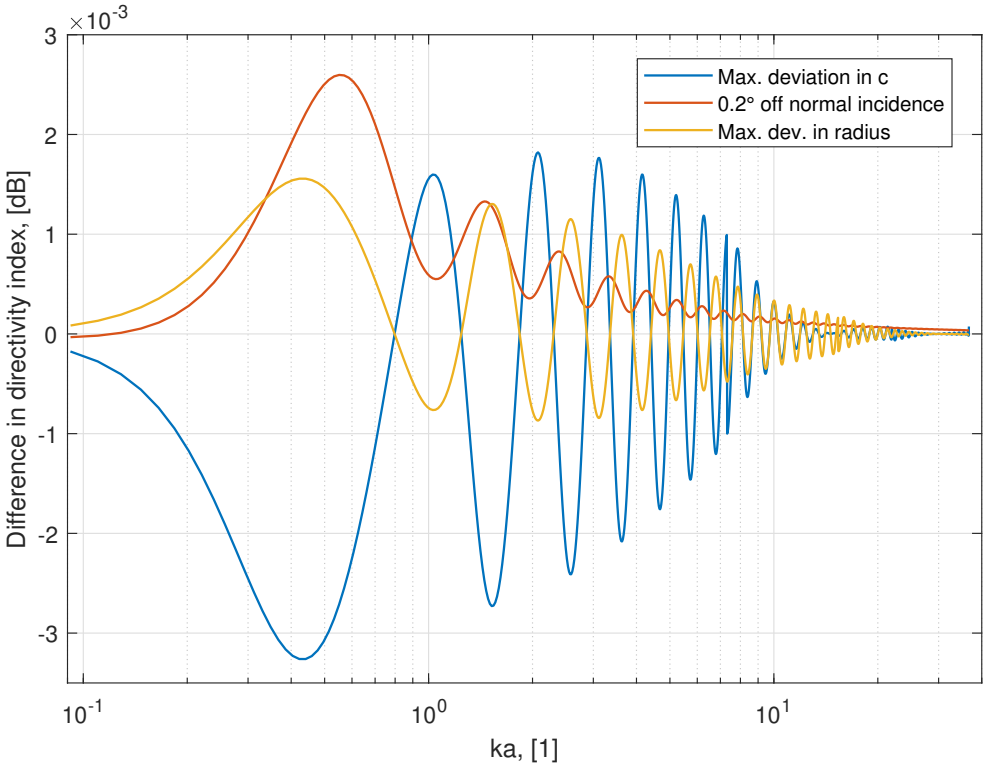


Figure 4.12: Difference in directivity index for three minor variable changes as simulated for the cylinder object: maximum deviation in the calculated velocity of sound, a shift in the normal incidence of 0.2° correlating to the range seen in measurements, and lastly the maximum value for the radius within the range of uncertainty found when measuring the constructed cylinder object. All differences are found by subtracting the value of the reference simulation from the simulation with the variable change.

As evident from Figure 4.12, the largest impact of these variable changes can be seen for the lowest $ka$ values. The difference in directivity index has the largest amplitude for the deviation in velocity of sound, represented by the blue curve, which at the most is a little more than $-3 \times 10^{-3}$ for a $ka$ value of 0.4-5. The amplitude of this curve then gradually decreases, until practically falling off completely when passing $ka$ values over 10.

The second largest amplitude is seen for the change in the angle of displacement for the normal incidence, which is illustrated in red. This reaches an amplitude of approximately $2.5 \times 10^{-3}$ for a $ka$ value between 0.5 and 0.6. This amplitude decreases even more sharply for increasing $ka$ values, stabilizing at just over zero for $ka$ values above approximately 7. Notably, this curve does not oscillate around zero; it is positive for all $ka$ values above 0.2.

For the difference in directivity index from using the maximum value of the radius of the cylinder, as given from the range of uncertainty when measured on the constructed cylinder object, this has its highest amplitude of about $1.5 \times 10^{-3}$ for a $ka$ value of a

little over 0.4. This amplitude slowly decreases for increasing $ka$ numbers, but retains a higher amplitude for the $ka$ values above 10 when compared to the other two curves.

One might note that the peaks and troughs for the deviation in velocity of sound and deviation in radius occur at similar $ka$ values but half a wavelength out of phase, while that of the incidence angle slightly off normal incidence has peaks and troughs at points that differ from the other two. The differences are all calculated by subtracting the value of the reference simulation from that of the simulations with the variable changes. The simulation for deviation in the velocity of sound is performed with the maximum value of the calculated velocities as found during the experimental measurements. The fact that the difference in directivity index for deviation in the velocity of sound and the deviation in radius are out of phase indicates that while an increase in the velocity of sound leads to a small increase in the directivity index for a given $ka$ value, an increase in the radius leads to a decrease in the directivity index for the same $ka$ value. These two deviations then, to a certain extent, cancel each other out, potentially masking the extent of their influence if they are not examined separately.

#### Best index approach

As for the measurements done on the cylinder and the box, the comparison of the different simulated directivity indices have been performed utilizing the "best index" approach. In other words, when calculating the difference between the results of the simulations, the difference in corresponding $ka$ values for given frequency points have been taken into account. The index point of the nearest $ka$ value existing for each point in the $ka$ values of the reference simulation have been found, and the difference has been calculated using these closest points for comparison. If not using the best index approach, then the differences as shown in all three curves in Figure 4.12 did not converge as they do for the upper $ka$ values.

### 4.2.2 Box

#### Directivity index

The simulations of the directivity index for a rigid box were performed by use of the toolbox called "EDtoolbox" [32], with the specifications detailed in Section 3.2.2. In the range of 100 Hz to 20 kHz, with a resolution of 10 Hz, and using the average value of the velocity of sound as calculated from the monitored environmental conditions when performing measurements on the box object, the directivity index was simulated both for the reference conditions, as well as with three minor variable changes in line with that simulated for the cylinder object. The resulting directivity index is shown in Figure 4.13.

Figure 4.13 shows that the simulated directivity index for the box increases steadily in the low ranges of $kl$ values, reaching a peak at a $kl$ value of approximately 6. It then quickly drops to a trough at a $kl$ value around 11, before steeply rising to another peak at a $kl$ value in the area of 16-17, which is remarkably similar to the $kl$ values of the

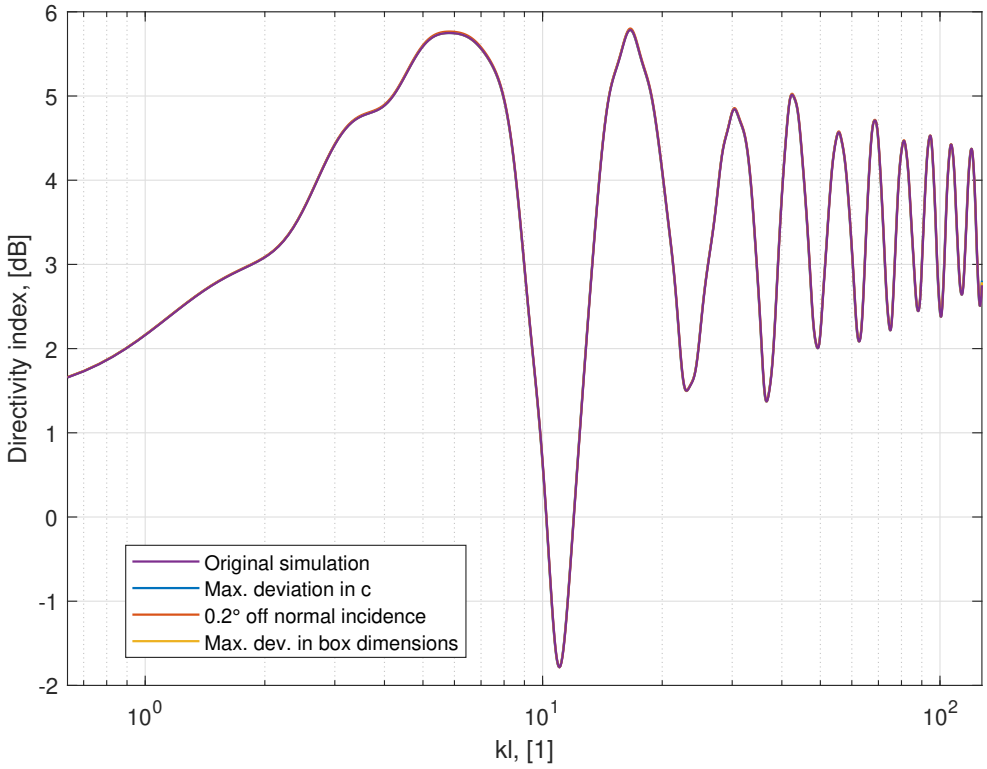


Figure 4.13: Simulated directivity index as a function of $kl$ number for the box object, including simulations with use of the maximum deviation in the velocity of sound, a 0.2 ° deviation in the normal incidence, and the maximum deviation in the dimensions of the box. Simulations are performed by use of the numerical solution ESIE.

first peaks and trough for the measured results seen in Figure 4.9. For what seen for the simulations, the highest values of the directivity index, at these two peaks, are a little under 6 dB, while the lowest value in the trough is nearly -2 dB, which is also of similar amplitudes as the measured directivity index. After these extreme values are reached, the simulated directivity index oscillates around a value of about 3.5 dB for the remaining $kl$ values, staying within the range of about 1.5 dB to 5 dB. As for the simulations done for the cylinder, the separate simulations done for the minor variable changes are not visibly distinguishable from one another in this figure.

### Difference in directivity index

In order to distinguish between the separate simulations, the difference in directivity index for the reference simulation and the three simulations with minor variable changes are plotted separately in Figure 4.14. In this figure, the blue line shows the difference from the reference simulation for the maximum deviation in velocity of sound, this time using the minimum value of the velocity of sound as that gave the largest deviation from the mean. The red line shows the difference in directivity index for the deviation in the normal incidence, using the value of 0.2° as that was found to be a realistic discrepancy, when going through the process of finding the necessary angle of displacement for the turntable to achieve normal incidence, before and after a completed measurement series for the box object. Lastly, the yellow line shows the difference in directivity index when comparing the simulation performed when using the maximum values of the dimensions of the box with the range of uncertainty as they were measured on the constructed box object, with the reference simulation.

The largest amplitude in the difference in directivity index is found for the deviation in velocity of sound, similarly to the simulations done for the cylinder. The amplitude of difference in directivity index has a maximum value of slightly less than -0.04 dB for a $kl$ value just over 10. The difference then oscillates around 0, with amplitudes decreasing slowly, staying less than 0.02 after $kl$ values of approximately 35.

The difference in directivity index for the deviation in the angle of normal incidence is positive throughout the entire $kl$ value range, as for the cylinder simulations. It increases slowly for the lower $kl$ values, staying less than 0.02 dB the entire range while oscillating slightly around 0.01 dB, until it reaches $kl$ values above 100 and starts increasing in amplitude, ending at nearly 0.03 dB for the highest frequencies.

The difference in directivity index for the maximum deviation in box dimensions oscillates around zero similarly to the difference for the maximum deviation in the velocity of sound. The amplitude of the difference for deviation in box dimensions, however, remains less than 0.03 dB for most values of $kl$, aside from three extreme values, where two troughs dip just below -0.03 dB, and the highest peak reaches a value of almost 0.035 dB.

For all three curves, there are large-scale oscillations occurring throughout the entire $kl$ range, but with larger amplitudes from $kl$ numbers 6 and above. There does, however, appear to be regions of destructive interference, where the amplitudes of the oscillations

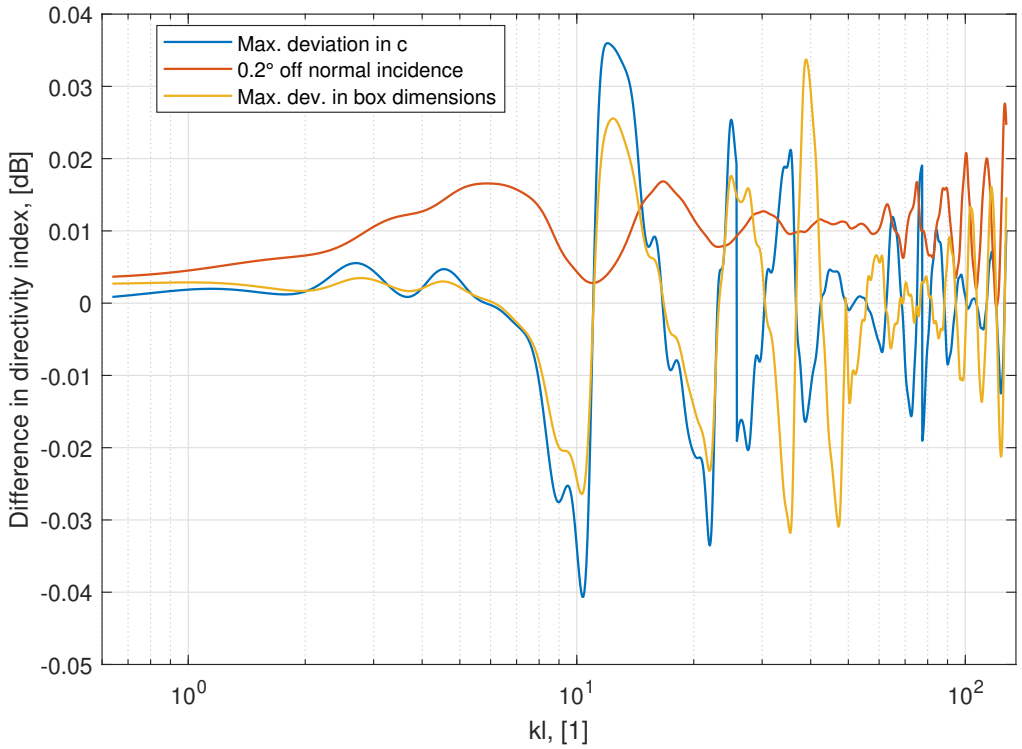


Figure 4.14: Difference in directivity index for three minor variable changes as simulated for the box object: Using the maximum deviation in velocity of sound, a deviation of 0.2° for the normal incidence, and for a maximum deviation in the dimensions of the box. The difference is calculated by subtracting the value of the reference simulation from the simulation with the variable change.

sharply decrease. For the curve relating to the deviation in velocity of sound, there seems to be such interference in the region around $kl$ numbers 45 to 60, and again for $kl$ numbers 100 and above. For the curve of deviation in angle of normal incidence, such interference is apparent from $kl$ number approximately 30 to 60. For the curve relating to deviation in box dimensions, the dampened amplitude appears from $kl$ number around 50 to 80. However, the dampened regions are not very clearly defined, and the start- and end points may be judged differently when evaluated by someone else.

### Best index approach

The simulations for the box have also undergone the consideration of which index points had the smallest horizontal distance between each other to ensure better comparison when calculating the difference in directivity index for the separate simulations. As for the cylinder simulations, the $kl$ values derived from the chosen frequencies of simulation are different from the reference simulation in the case of the deviation in velocity of sound and deviation in box dimensions. It remains the same, however, for the deviation in angle of normal incidence.

Similarly to the cylinder simulations, the use of the best index approach has had an effect on the difference in directivity index mainly for the higher frequencies. The curves of the deviation in velocity of sound and that of the deviation in box dimensions both see amplitudes significantly reduced for $kl$ values above 25 and 50, respectively. The interested reader can see an illustration of the difference calculated without the use of the best index method in Figure B.3 in Appendix B.

While the simulated directivity index for the deviation in velocity of sound is pointed out as the one that gives the largest amplitude of discrepancy when compared to the reference simulation, this is a consequence of the method used. The best index approach limits the effect of comparison of curves with different values on the x-axis, it does not give a perfect comparison. In the case of the curve for the deviation in velocity of sound, there is actually an extremely good fit between the curve and that of the reference simulation. This is illustrated in Figure 4.15.

This fit is present also at the maximum value of the difference in directivity index. The discrepancy in the $kl$ value leads to comparing directivity index values of different value, due to the incline of the curve. Looking at the curves, however, it is easy to see that the difference is in fact nearly indetectable compared to the magnitude of difference between the reference curve and the remaining curves. Realistically, the difference in directivity index for the deviation in velocity of sound is approaching zero, and hence deviation in velocity of sound is not actually the factor giving the largest amplitudes of difference in directivity index for simulations on the box object. For the box, the deviation in box dimensions gives the largest amplitude of difference in directivity index at lower $kl$ numbers, up to about 50, while deviation in the angle of incidence gives the largest amplitude for $kl$ numbers above this.

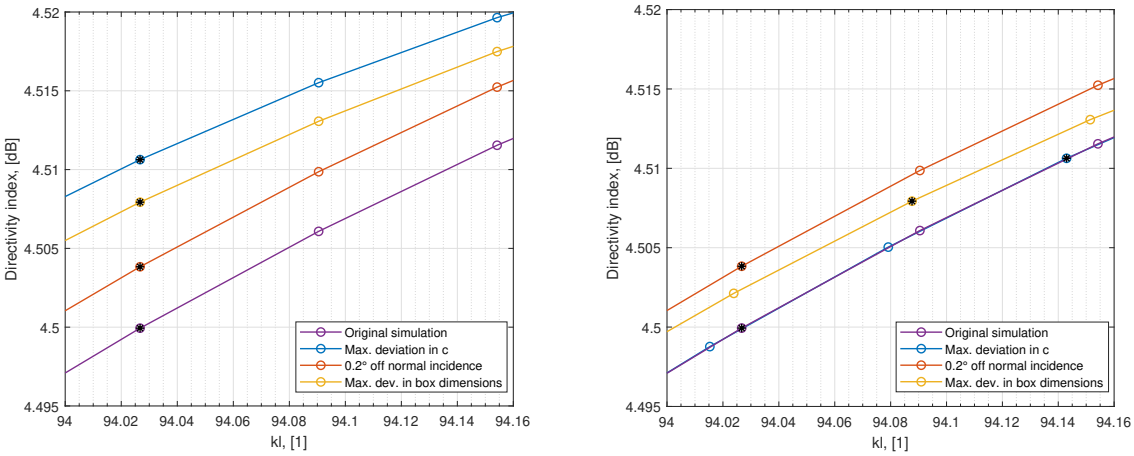


(a) Using the same $kl$ values for all curves.

(b) Using individual $kl$ values for the curves.

Figure 4.15: Directivity index simulated for the box object with four different conditions, showing three different frequency values for all curves. The same frequency value (index point) is marked on all curves in black.

## 4.3 Summary and further discussion

The variable changes that were studied through measurements were a change in loudspeaker used for measuring, whether the ventilation was switched on or off, repositioning of the microphone, and repositioning of the loudspeaker. Additionally, an uncertainty in the velocity of sound, the angle for normal incidence, and the dimensions of the scattering objects were studied through simulations. Following is an extension of some of the points that have been discussed so far in this chapter.

### 4.3.1 Measurements

Through the measurements done on the cylinder, the uncertainty from a change in the loudspeaker used to do the measurements of the directivity index has a magnitude of less than 0.6 dB for most of the frequency range, including both the difference between the means and the difference between the max deviations from the mean, as seen in Figure 4.6. For the lower frequencies loudspeaker #2 gives a higher directivity index, up until a $ka$ value of about 10, when loudspeaker #1 gives a higher value. For $ka$ values above 5-6 the difference in directivity index remains less than $\pm$ 0.2 dB.

The measurements done on the box reveal values of the same magnitudes for the difference in directivity index when changing the loudspeaker. For the box there is a higher difference for the lower frequencies, as seen in Figure 4.10, with the difference in the mean values being a little over 0.6 dB for the lowest $kl$ values, while the difference between the maximum deviations reach a magnitude of over 1.2 dB. For most of the $kl$ value ranges, however, it is far less than this, remaining mostly below $\pm$ 0.2 dB for $kl$ values above 20.

As can also be seen in Figure 4.10, the difference in directivity index when comparing the measurements done with the ventilation switched off and on remains less than 0.5 dB for the entire frequency range apart from the very lowest $kl$ value. For most of the range the difference between the means is less than $\pm$ 0.05 dB. The difference is positive for low frequencies, meaning that the directivity index is higher for the ventilation switched off than for the ventilation switched on, up until $kl$ value approximately 15 where it first starts dipping beneath zero. After this the difference oscillates around 0. The difference between the maximum deviations follows a similar trend, staying below 0.2 dB for $kl$ values over 3, and dipping below 0.1 dB after $kl$ value about 15. It remains low for increasing frequencies, but has a peak at the highest range of $kl$ values beyond 100.

While the author expected that keeping the ventilation on would affect the measurement data quite a lot due to increased noise, the noise measurements and noise floor estimate in Figure 4.7 revealed that the difference between having the ventilation on or off was minor. While having the ventilation on revealed some higher levels of noise at the lower frequencies, this was mostly below the lower frequency cutoff found from the 30 dB SNR estimate. It was also expected that the environmental conditions would remain noticeably more stable with the ventilation on, but as can be seen in Figure 4.2, this was not discernible.

The third subplot in Figure 4.10 shows the difference in directivity index as estimated by comparing the measurement series done with the microphone kept stationary, and measurement series where the microphone (along with the box object it was mounted in) was repositioned. The figure shows the absolute value of the difference. As can be seen, the difference in the mean remains small throughout the entire illustrated frequency range, with values below 0.2 dB. The difference between the maximum deviations is slightly larger, starting around 0.4 dB for the lowest frequencies and approaching 0.5 dB for the highest frequencies. For the most part it stays below 0.3 dB, however.

For repositioning of the loudspeaker, shown at the very bottom of Figure 4.10, the difference between the means starts just above 0.2 dB but remains below this for $kl$ values above 2. The difference between the maximum deviations starts high at almost 0.7 dB, decreases steadily then increases again with a peak around $kl$ value 11, before finally remaining approximately 0.2 dB or lower for $kl$ values above this.

In the directivity factors illustrated in Figures 4.3 and 4.7, one can observe a region of irregularities in the results from loudspeaker #2 for the $ka$ values 4.5-8 and $kl$ values 17-25. These ripples, seen both in the normal incidence measurement and the averaged measurements across all angles of incidence, are suspected to indicate a resonance frequency area for this loudspeaker. When converting the $ka$ and $kl$ values, it is not surprising to find that the frequency in hertz falls in the same approximate range: 2.6-4.0 kHz. With the same behavior being observed for both scattering objects, it seems even more likely to be an inherent quality of the loudspeaker itself. It does not, however, coincide with the resonance frequencies that are given for the loudspeakers in Appendix C.

### Windowing function

The large-scale oscillations seen in Figure 4.7 and 4.9 were most likely caused by the geometry of the box object. The same behavior was seen in the simulated directivity index as shown in Figure 4.13. The small-scale oscillations seen in Figure 4.8 were found to probably be caused by unwanted reflections being included in the windowed data used during the post-processing, as a shorter window resulted in these being greatly reduced, as seen in Figure 4.9. While there are small-scale oscillations present in the measurements done on the cylinder object as well, seen in Figure 4.5, an attempt at using a shorter time window did not result in these being reduced. Hence, it is unlikely that these are caused by unwanted reflections being included along with the direct sound in the post-processing.

In addition to the length of the time window, it was also tested whether the use of a two-sided Hanning window could change the results. This was done by adding a taper-in for the first 10 values of the window, and repeating the post-processing on the measurement data from the cylinder. No difference was found for this change, and as such it was not implemented.

### Cutoff values

While the frequencies used during measurements span the same range, 0 Hz to 24 kHz, the cutoff values for the different loudspeakers and the different scattering objects are slightly different based on the signal-to-noise ratio, as indicated in Table 4.1. This, however, does not take into account the limitations of the transducers used for the measurements. As can be seen in the tables in Appendix C, loudspeaker #1 has a recommended frequency range from 3 kHz to 25 kHz, while loudspeaker #2 is stated to feature use in frequencies between 250 Hz and 25 kHz. Based on Figures 4.3 and 4.7, the cutoff value for loudspeaker #2 was estimated at 111 Hz and 117 Hz respectively, which is below the range of recommended use. As cutoff values of 237 Hz and 267 Hz found for loudspeaker #1 have been used for the cylinder and box measurements respectively, and nothing below this is shown in the figures, it approximately coincides with the given frequency range for loudspeaker #2. However, this is far below the recommended lower limit of 3 kHz for the loudspeaker, but from a signal-to-noise ratio perspective, this does not seem to be a problem. Regardless, the difference in directivity index found for comparison of measurements done with the two different loudspeakers in Figures 4.6 and 4.10 show larger amplitudes of difference for the lower frequencies, and this could be tied to loudspeaker #1 being used beyond its recommended frequency range.

No upper cutoff values were found through signal-to-noise ratio considerations for loudspeaker #1, but loudspeaker #2 saw a cutoff at approximately 23.9 kHz for the cylinder measurements and 21.9 kHz for the box measurements. This could be tied to the different voltages (listed in Table A.3) measured across the power amplifier when using the two different loudspeakers; the measurements are not calibrated, so different sound pressure levels are generated by the two. This is visible in Figures 4.3 and 4.7 by the vertical difference between the results given by the two loudspeakers. Another thing

one might consider is how directive the loudspeakers may become at higher frequencies, and that the difference in scattering object geometry may affect the signal strength seen at different points in the higher frequency region. It should also be noted that as seen in Appendix C, the microphone has a recommended frequency range of 3.15 Hz to 20 kHz, meaning it may have behavior in the higher frequency regions that limits the reliability of the measured data.

The signal-to-noise ratio considerations in Figures 4.3 and 4.7 may also not be sufficiently accurate for some intents; if the criteria is for the noise to make up no more than 1/1000 of the measured signal energy, adding 30 dB to the estimated noise floor is not sufficient. As seen in Equation 2.13, when the measured signal consists of both noise and signal, the difference must be slightly larger than the desired SNR. However, for the values utilized here, this difference is not very large, and for that reason has been neglected. While somewhat exact cutoff values have been found, they are viewed more as estimates found to simplify figures and to avoid including uninteresting regions of non-reliable data, than as exact boundaries between reliable and unreliable data.

On that same note, it should also be mentioned that the cutoff values have been calculated based on the intersection between the directivity factor numerator and denominator of only one example measurement series and for this reason, there is also no exact estimate of the uncertainty of this cutoff value. However, as has been pointed out, this value is not considered to be a precise distinction between reliable and unreliable data, but rather as a guideline for limiting the range of $ka$ and $kl$ values that is focused on in the figures.

The post-processing for the box measurements also saw a change in the time window used. Based on this change, the cutoff value calculation was repeated, and it was found that the lower cutoff values for both loudspeakers had shifted slightly downward in the frequency range, to values of 264 Hz and 108 Hz for loudspeakers #1 and #2 respectively. Keeping in mind the nature of the cutoff values as guidelines, and the extent of the shift, it has not been implemented in the axis limits for the figures presented as it was deemed negligible.

### Limitations for cylinder measurements

The scattering measurements performed for the cylinder object had a limited extent when compared to those performed for the box object, as is evident in the overview of measurement setups presented in Table 3.1. The effect of toggling the ventilation on as opposed to off, as well as the effect of repositioning the microphone with the scattering object, and repositioning the loudspeaker, was not examined for the cylinder object. In the case of microphone repositioning this is strongly linked to what was practically possible; positioning the cylinder object with the combination of ceiling mounting and turntable mounting required more than one person to execute, and repeating this for several series was not deemed practicable for such a large construction.

The ambient air pressure was also not monitored during the cylinder object measurements, and this is a source of uncertainty. While temperature seems to have the largest

impact on the velocity of sound out of the three monitored environmental conditions, the assumption of the air pressure's value is a distinction to be aware of.

Comparing the difference in directivity index for a change of loudspeaker for the two scattering objects, as seen in Figure 4.6 and the topmost part of Figure 4.10, they are of comparable magnitudes, staying mostly below 0.5 dB, except for in the lower frequency regions, where the box measurements show a higher difference between the two loudspeakers. The trends are the same, however, with loudspeaker #2 giving a higher directivity index for the lower frequencies, with the difference declining for increasing $ka$ and $kl$ values, before finally oscillating around zero.

It is difficult to say whether comparing the other measurement setups performed for the box would result in different conclusions for the cylinder object, but it would not be surprising if the trends in the results were similar to that seen for the box object, but with smaller differences for the lower frequencies as seen for the comparison measurements done with two different loudspeakers.

Lastly, it is uncertain to what extent the qualitative nature of the results seen here, with change in loudspeaker being the largest source of difference in directivity index, applies to other anechoic chambers. The specific transducers used are likely to have a large effect on this result. For the sake of repeating a measurement series, it is not certain that the discrepancy between other loudspeaker types would be of the kind examined here. For users of anechoic chambers it might then be worth to look into the extent of uncertainty from relevant variables in their locations, especially if assumptions have been made about these in the past and are maintained simply by habit. Variables are also subject to change, as seen for instance in the temperature variations (leading to changes in the velocity of sound) from seasonal changes, as found when comparing Figures 4.1 and 4.2.

### 4.3.2 Simulations

Simulations were performed by use of the analytic solution for an infinitely long, rigid cylinder, and by use of a numerical solution toolbox utilizing the ESIE method for the box. A change in three variables, being deviation in velocity of sound, a displacement angle off normal incidence, and a deviation in object dimensions, was simulated and compared to a reference simulation without these changes. The magnitude of the changes was in accordance with the uncertainty seen when performing experimental measurements on the two different objects. The difference in directivity index as found by simulations were within approximately $\pm\, 3 \times 10^{-3}$ dB for the cylinder object, with deviation in the velocity of sound contributing the most up to a $ka$ value of about 10, after which the deviation in cylinder radius contributes the most. For the box object the difference is within a range of approximately $\pm$ 0.04 dB, also with the deviation in velocity of sound contributing the most at lower frequencies. However, more careful study of the curves revealed that there was in reality a nearly indetectible difference between then simulated reference results and those of the deviation in velocity of sound. In conclusion, for the box, the simulations indicated that for $kl$ numbers up to 50, the

largest difference in directivity index originated from the deviation in box dimensions, while for $kl$ numbers above this the deviation in angle of incidence gave the largest difference.

### Comparison with measured results

Comparing the simulated directivity index for the cylinder as seen in Figure 4.11 with that found for measurements in Figure 4.5, there are similar trends with the directivity index increasing rapidly from the low frequencies, and oscillating around a value. However, that is a constant value in the simulations, while the results from the measurement showed the directivity index oscillating about an increasing value for increasing frequency. This particularly seems to be the case for $ka$ values above 20, where one can see a rapid increase in the value of the measured directivity index. This could be an expression of how the directivity of loudspeakers tend to increase for higher frequencies, but perhaps even more so for the directivity of the microphone. Microphones of the kind used here are increasingly directive for higher frequencies [57], meaning that for angles other than the normal incidence the sound pressure level will be estimated as too low compared to what it realistically is, making the average value for all angles lower than its realistic value. As a consequence, the denominator in the calculation of the directivity factor is too low, making the directivity factor, and hence directivity index, appear to have a larger value than it actually does. This gives the directivity index it an increasingly too large value for increasing frequencies.

The measurements also showed small-scale oscillations, which did not change with a shortened time window, indicating that it was not caused by unwanted reflections. Since the effect is also observed in the simulations, it then seems to be expected behavior for scattering on a cylinder object.

The simulations for the box object, as seen in Figure 4.13, see the same trends as those measured, shown in Figure 4.9. The large-scale oscillations have very similar shapes, especially for the first four peaks and troughs. Similarly to the cylinder measurements, the measured values for the box object seem to oscillate around a value that increases for increasing frequencies, a behavior which is not present in the simulations. This may then, as mentioned, be a result of the microphone becoming increasingly directive at higher frequencies.

### Limitations

There are certain limitations in place for the simulations. The properties of the loudspeakers and microphone are not taken into account, and they are assumed to be points, which is not a realistic representation. In the cylinder simulations the incident wave is assumed to be a plane wave, while this is not likely to be the case experimentally. For the box simulations a spherical wave is utilized. This is a source of discrepancy between the two simulations.

For the simulations of the cylinder object, the magnitude of the directivity index differ-

ence recorded is a tenth of that found for the box object, seen in Figures 4.12 and 4.14. This may be caused by the use of an analytical solution as the basis for the simulation, but it is hard to say without further study. The solution for the ideal infinitely long, rigid cylinder also does not take into account the presence of edge diffraction, though time windowing to isolate the direct sound will limit some of the influence of this. Internal resonances in the constructed cylinder may also contribute to realistically larger uncertainties than what is indicated in Figure 4.12.

The simulation of the box object required a careful weighing of required calculation time against desire for precision. As discussed in Section 3.2.2, the author of the toolbox recommends at least three discrete points along the longest side of the scattering object per wavelength for the highest frequency simulated, and after testing several values, a decision was made to use less than the recommended number, since the directivity index appeared to converge for fewer discrete points. According to the recommendation, simulating to an upper limit of 20 kHz would correspond to 68 discrete points along the longest dimension of the box. Instead, 47 discrete points were used. The directivity index as found for the two test frequencies with 68 discrete points was used as the reference for determining for what number of discrete points the directivity index converged, but whether or not this is an adequate reference is undetermined.

### 4.3.3 Concerning both measurements and simulations

#### The $ka/kl$ value problem

For all comparison of directivity factor or index, both for measurements and simulations, the best index approach has been used to make sure that comparison is done between points that are as close to each other in $ka$ or $kl$ value as possible. The frequency resolution was found to affect how much improvement could be gained from use of the best index approach. However, as seen for the simulations of the box object, this method has its drawbacks. It is readily illustrated in Figure 4.15 that this way of comparing directivity indices can give an erroneous impression of the relationship between different results. It is not investigated whether the use of an average value for the velocity of sound affects the placement of the points significantly, and searching for better methods of comparing the curves using for instance regression tools were deemed beyond the scope of this thesis.

#### Angular resolution

Simulations for the cylinder object found that a higher angular resolution than 4° did not significantly change the values of the directivity index. This resolution was therefore used in the simulations and measurements for the cylinder object. For the box simulation, finer resolutions gave changes in the directivity index in the order of 1/1000 for two test frequencies, and due to the increase in runtime, it was deemed unproductive to implement a finer resolution. Steps of 4° were then used for the box simulations and measurements as well.

# Chapter 5

# Conclusion

## 5.1 Comments on results

The effect of seven variable changes was studied for the impact on directivity index, using both experimental measurements and simulations for a cylinder and a box object. The variables studied were a change in loudspeaker, switching the ventilation on and off, repositioning the microphone with the scattering object, repositioning the loudspeaker, a deviation in the velocity of sound, a deviation in the angle of normal incidence, and lastly a deviation in the dimensions of the scattering object.

Out of the seven variables, the first four were studied through measurements, and found to give changes in the directivity index within the range of 0.5 dB for most of the frequency range. This includes both the difference in the mean and the difference in the maximum deviation of the directivity index. The magnitude of difference is slightly larger for that of a change in loudspeaker, which is seen as the largest contributor to difference in directivity index for the lower frequencies, whilst for $kl$ values above 20 the repositioning of particularly the microphone with the scattering object has the largest impact. The differences generally stay well below the typical order of 1 dB difference for repeated measurements in acoustics [13].

The directivity index as found from measurements showed both small-scale and large-scale ripples, where the small-scale ripples for the box measurements could be explained by unwanted reflections being included in the time window during post-processing. The large-scale ripples of both the cylinder and the box measurements seem to be caused by the object geometry, as they are found in the simulated directivity indices as well.

The latter three variables were studied through simulations, where the results for the cylinder, modelled as an ideal infinitely long, rigid cylinder, stayed below approximately $\pm\, 3 \times 10^{-3}$ dB. The results for the box object were within approximately $\pm$ 0.04 dB. For the cylinder simulations the change in velocity of sound was the largest contributor to difference in the lower frequency range, while for values above about $ka = 10$, the deviation in cylinder radius had the largest contribution. For the box simulations the

deviation in box dimensions had the largest contribution for $kl$ values below 50, while the deviation in angle of incidence contributed the most above this.

## 5.2 Further work

The work done in this thesis could be expanded upon in several ways. The variable changes that were studied through measurements for the box object could be studied for the cylinder as well, perhaps aside from repositioning the microphone with the scattering object due to its difficulty in handling.

One could also study the effect of different window functions on the measured results after post-processing. While a half Hanning window might be appropriate, the length has not been optimized in the work done here aside from on a very rudimentary level.

The simulations of the cylinder object could be elaborated upon by use of a numerical method as opposed to an analytic solution. Realistically the constructed object is quite far from an infinitely long, rigid cylinder, despite its construction being as long as possible to reduce the impact of this discrepancy. Use of a numerical solution might then give different results.

When calculating the difference in the directivity index upon comparison of different measurement setups, the problem of directivity index values being correlated to different $ka$ or $kl$ values has been discussed throughout this work. For the sake of a more precise calculation of this difference, it could be beneficial to compare these curves by use of regression tools. In the case of the simulations for the box object, the deviation in velocity of sound was found to be the largest source of difference in directivity index, but a closer look at the curves revealed that this was due to the difference in $kl$ values and not due to a difference between the curves. Use of regression tools may then largely affect the findings of this thesis.

A more in-depth study of the statistical methods commonly used to treat uncertainty estimation could make it easier to compare the different results. Further study of the methods outlined in ISO standard 98-3:2008 (*Guide to the expression of uncertainty in measurement*) [12] could also benefit this purpose.

Lastly, though beyond the scope of this thesis, it must be mentioned that the work can be expanded upon by looking into the uncertainties attached to the simulations. No attempt has been made to estimate this, but for the sake of comparison with measured data, and in particular if comparing several different simulation methods, it would be largely helpful.

# Appendix A

## A.1 Cylinder dimensions

The measured dimensions of the cylinder object is shown with a combined uncertainty from standard deviation and measurement uncertainty is given in Table A.1.

Table A.1: Dimensions for the cylinder including a combined uncertainty of the standard deviation of the range and the instrumental error.

| **Dimension** | **Value** |
|---|---|
| Height from lower end to microphone [cm] | 179.8 ± 0.1 |
| Radius [mm] | 200.43 ± 0.12 |

## A.2 Box dimensions

An illustration of the box object and its dimensions is shown in Figure A.1. The measured dimensions of the sides of this box are given in Table A.2, where the numbering of the sides follows the convention set in Figure A.1.

Table A.2: Dimensions for the box including a combined uncertainty of the standard deviation of the range and the instrumental error.

| **No.** | **Height, h [mm]** | **Width, w [mm]** | **Depth, d [mm]** |
|---|---|---|---|
| 1 | 329.56 ± 0.08 | 329.55 ± 0.07 | 390.56 ± 0.08 |
| 2 | 329.47 ± 0.07 | 329.20 ± 0.08 | 390.78 ± 0.06 |
| 3 | 329.53 ± 0.08 | 328.74 ± 0.08 | 390.91 ± 0.08 |
| 4 | 329.20 ± 0.07 | 328.65 ± 0.09 | 390.67 ± 0.06 |
| Average | 329.4 ± 0.2 | 329.0 ± 0.4 | 390.7 ± 0.2 |

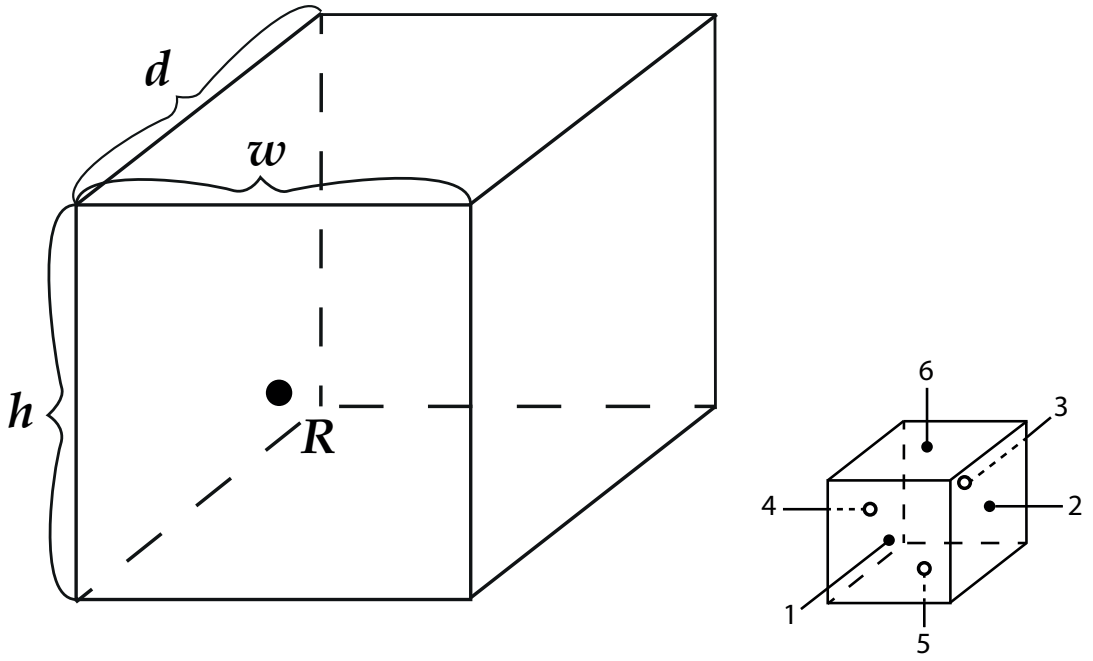


Figure A.1: Figure showing the structure and defining variable names for dimensions of the box object. Additionally there is a smaller figure defining the numbering for the surfaces, utilized in the measurements of the dimensions. The receiver is mounted in the front facing panel.

## A.3 Equipment list

The equipment used for all experimental measurements is shown in Table A.3. Note that the same two loudspeakers are used both for the cylinder object sound scattering measurements and the box object ones. However, the barometer, analog scale, web camera, flashlight, and digital voltmeter were only used during the box object sounds scattering measurements.

Table A.3: Equipment list for sound scattering measurements performed on cylinder and box objects in the anechoic chamber.

| **Equipment** | **Manufacturer** | **Type** |
|---|---|---|
| Microphone | Brüel & Kjær | Free-field 1/2" 4190 |
| Loudspeaker #1 | SEAS | H615 Dome Tweeter (2.34 V during measurements) |
| Loudspeaker #2 | AuraSound | NSW1-205-8A 1" (3.31 V during measurements) |
| Microphone pre-amplifier | Norsonic | Nor 1201 |
| Barometer | Brüel & Kjær | UZ 0003 |
| Thermometer/hygrometer | CMOSens | SHT1x (RH/T) |
| Microphone amplifier | Brüel & Kjær | 1708 |
| Power amplifier | Rotel | RB-1552 MKII |
| AD/DA converter | Lynx Studio Technology, Inc. | Aurora Lynx USB |
| Turntable | Norsonic | Nor 265 |
| Laser meter | DeWALT | DW087 |
| Level meter | RIDGID | 385 Magnetic |
| Laser distance meter | Leica | DISTO X310 |
| Digital caliper | Mitutoyo Corp. | CDN-50C |
| Analog caliper | Ironside | 150 mm |
| Analog scale | MIKRO Döft ges. gesch. | DÖFT 800 |
| Web camera | Logitech | C920e HD Webcam |
| Flashlight | LED LENSER | X7R |
| Analog voltmeter | PROMAX | MVT-950 |
| Digital voltmeter | Agilent | U1231A |
| Various cables, tape, screwdrivers, connection rack | N/A | N/A |
| Cylinder object under testing | In-house built | PVC pipe, absorbent material filling |
| Box object under testing | In-house built | Wooden plates, absorbent material lining, hollow core |
| Program for measuring | AFMG Technologies | EASERA 1.2.16.4 |
| Program for post-processing | MathWorks Inc. | MATLAB R2018a |

# Appendix B

## B.1 Environmental conditions

The local variations of environmental conditions that were monitored during the sound scattering measurements performed on the cylinder object are shown in Figure B.1, including the monitored values of temperature in (a), humidity in (b), and calculated velocity of sound in (c).

The local variations of environmental conditions as monitored during sound scattering measurements on the box object are shown in Figure B.2. The temperature is given in (a), the humidity in (b), air pressure in (c), and the calculated velocity of sound in (d). This is shown for an example measurement setup along with the average value, and other measurement setups have similar results.

## B.2 Difference in directivity index

The difference in directivity index for three variable changes as simulated for the box object is shown in Figure B.3. The difference is calculated without using the best index approach, for a deviation in the velocity of sound, a deviation in the angle of normal incidence, and a deviation in the dimensions of the box object.

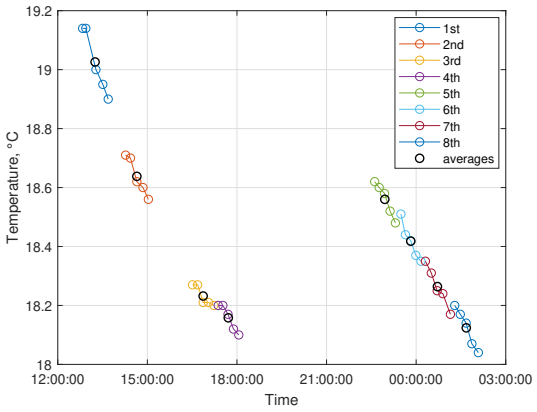


(a) Temperature

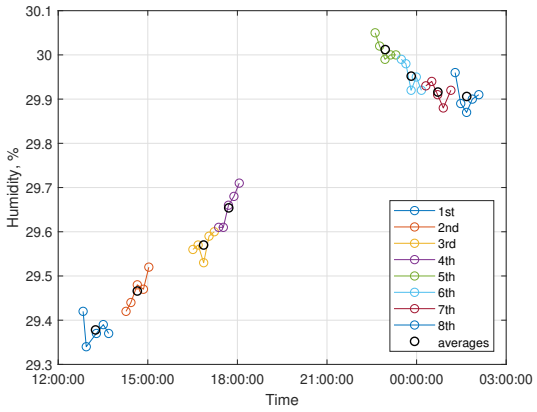


(b) Humidity

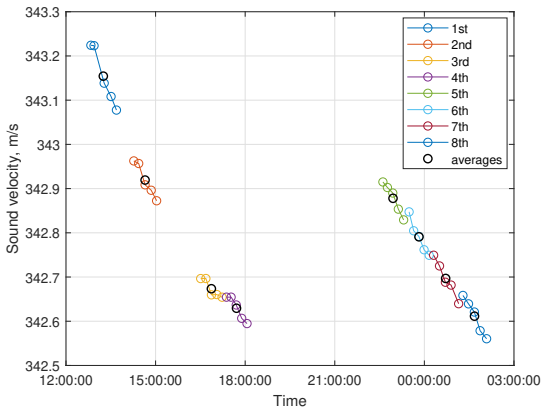


(c) Velocity of sound

Figure B.1: Local variations of environmental variables that were monitored during sound scattering measurements performed on the cylinder object; (a) temperature, (b) humidity, and (c) calculated velocity of sound from the monitored variables. Shows each of the logged values for all eight measurement series performed on the cylinder object.

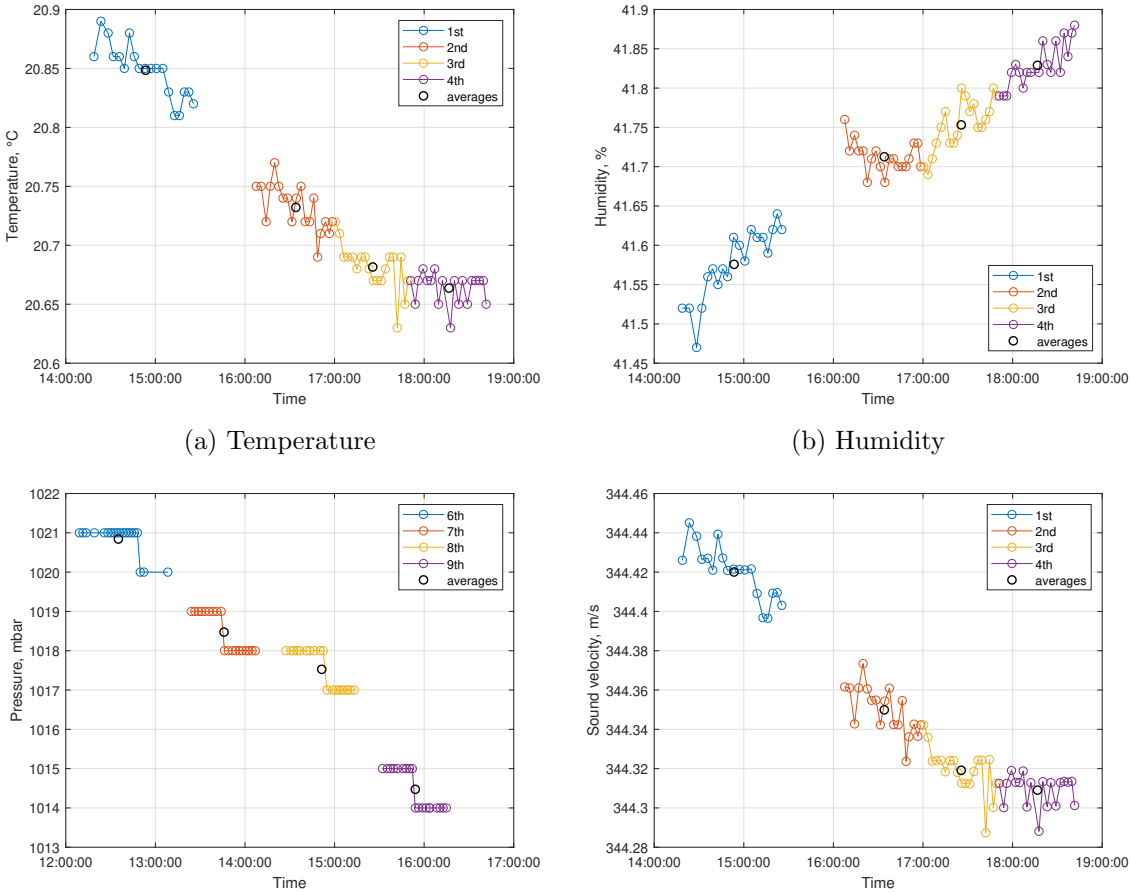


(a) Temperature

(b) Humidity

(c) Pressure

(d) Velocity of sound

Figure B.2: Local variations of environmental variables that were monitored during sound scattering measurements performed on the box object; (a) temperature, (b) humidity, (c) pressure, and (d) calculated velocity of sound from the monitored variables. Shows each of the logged values for four measurement series performed on the cylinder object for one measurement setup. Note that the pressure is shown for the next four measurement series, in order to showcase a more typical behaviour as the pressure hardly had any variation for the first four measurement series shown in the other figures.

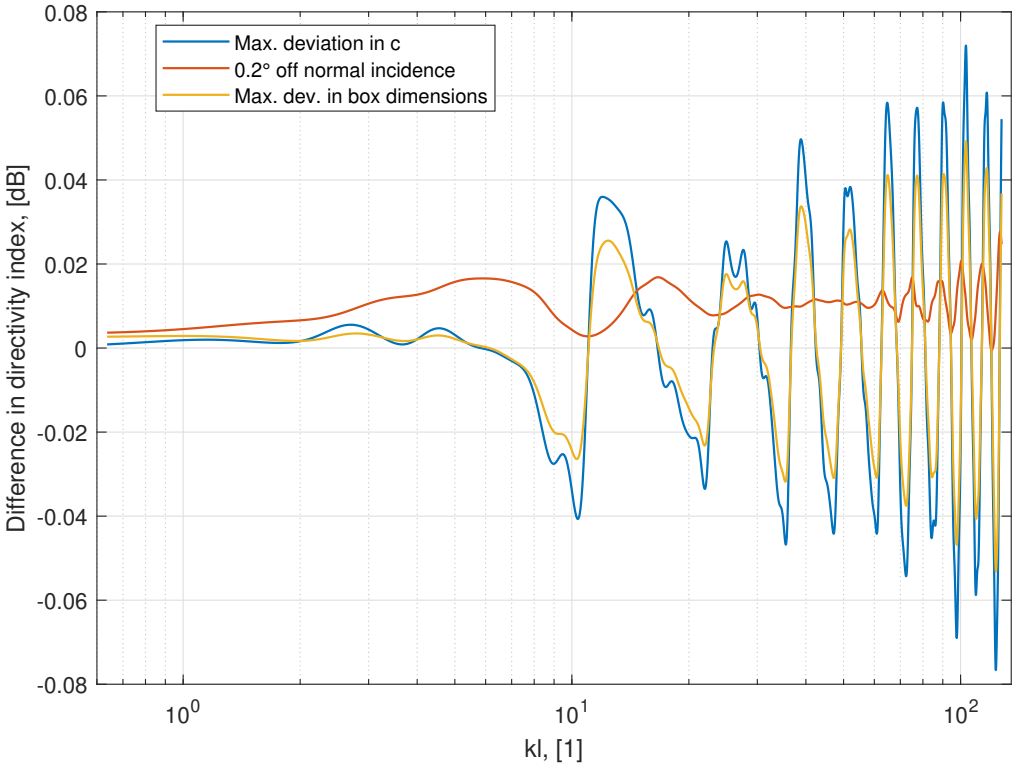


Figure B.3: Difference in directivity index for three minor variable changes as simulated for the box object: Using the maximum deviation in velocity of sound, a deviation of 0.2° for the normal incidence, and for a maximum deviation in the dimensions of the box. The difference is calculated by subtracting the value of the reference simulation from the simulation with the variable change, without using the best index approach.

# Appendix C

## C.1 Microphone data

Information about the microphone utilized as given by the data sheet [59] can be found in Table C.1.

Table C.1: Selected microphone specifications from data sheet produced by manufacturer.

| **Specification** | **Value** |
|---|---|
| Size | 1/2” |
| Recommended frequency range [Hz] | 3.15 - 20 000 |
| Dynamic range [dB] | 15 - 148 |

## C.2 Loudspeaker data

Information about loudspeaker #1 can be found in Table C.2, while equivalent data for loudspeaker #2 is shown in Table C.3. The information is collected from the data sheets for loudspeaker #1 [60] and loudspeaker #2 [61] respectively.

Table C.2: Selected specifications for loudspeaker #1 from data sheet produced by manufacturer.

| **Specification** | **Value** |
|---|---|
| Radiating piston area [$cm^2$] | 7.0 |
| Recommended frequency range [Hz] | 3 000 - 25 000 |
| Resonance frequency [Hz] | 1800 |

Table C.3: Selected specifications for loudspeaker #2 from data sheet produced by manufacturer.

| **Specification** | **Value** |
|---|---|
| Radiating piston area [$cm^2$] | 5.31 |
| Recommended frequency range [Hz] | 250 - 25 000 |
| Resonance frequency [Hz] | 220 |

# Bibliography


[1] Lawrence E. Kinsler, Austin R. Frey, Alan B. Coppens, and James V. Sanders. *Fundamentals of Acoustics*. John Wiley & Sons, Inc., 4th edition, 2000. ISBN 978-0471-84789-2.

[2] Allan D. Pierce. *Acoustics, An Introduction to Its Physical Principles and Applications*. Springer Nature Switzerland AG, 3rd edition, 2019. ISBN 978-3-030-11213-4. doi: 10.1007/978-3-030-11214-1.

[3] Thomas D. Rossing, editor. *Springer Handbook of Acoustics*. Springer-Verlag Berlin Heidelberg, 2nd edition, 2014. ISBN 978-1-4939-0754-0. doi: 10.1007/978-1-4939-0755-7.

[4] Finn Jacobsen and Peter Møller Juhl. *Fundamentals of General Linear Acoustics*. John Wiley & Sons, Inc., 2013. ISBN 9781118636319.

[5] Marshall Long. *Architectural Acoustics*. Elsevier Science & Technology, 2nd edition, 2014. ISBN 9780123982582.

[6] John P. Bentley. *Principles of Measurement Systems*. Pearson Education Limited, 4th edition, 2005. ISBN 978-0-13-043028-1.

[7] Fabian Brinkmann, Lukas Aspöck, David Ackermann, Steffen Lepa, Michael Vorländer, and Stefan Weinzierl. A round robin on room acoustical simulation and auralization. *The Journal of the Acoustical Society of America*, 145(4):2746–2760, 2019. doi: 10.1121/1.5096178. URL `https://asa.scitation.org/doi/10.1121/1.5096178`.

[8] Fabian Brinkmann, Lukas Aspöck, David Ackermann, Rob Opdam, Michael Vorländer, and Stefan Weinzierl. A benchmark for room acoustical simulation. concept and database. *Applied Acoustics*, 176(107867), 2021. doi: 10.1016/j.apacoust.2020.107867. URL `https://www.sciencedirect.com/science/article/pii/S0003682X20309725#!`

[9] U. Peter Svensson, Andreas Asheim, and Sara R. Martín. Sound propagation through an aperture with edge diffraction modeling. *Acoustical Society of America*, 141(5):3784, 2017. doi: 10.1121/1.4988332. URL `https://asa.scitation.org/doi/10.1121/1.4988332`.

[10] Pascal Dietrich. *Uncertainties in Acoustical Transfer Functions: Modeling, Measurement and Derivation of Parameters for Airborne and Structure-borne Sound*. Logos Verlag Berlin GmbH, 2013. ISBN 978-3-8325-3551-3.

[11] Ingolf Bork. A comparison of room simulation software - the 2nd round robin on room acoustical computer simulation. *Acta Acustica*, 86(6):943–956, 2000.

[12] International Organization for Standardization. *Guide 98-3 Uncertainty of measurement, Part 3: Guide to the expression of uncertainty in measurement (GUM:1995)*, 2008.

[13] Gerhard Müller and Michael Möser, editors. *Handbook of Engineering Acoustics*. Springer-Verlag Berlin, 2013. ISBN 978-3-540-24052-5. doi: 10.1007/978-3-540-69460-1.

[14] Leo L. Beranek and Tim Mellow. *Acoustics: Sound Fields and Transducers*. Elsevier Science & Technology, 2012. ISBN 9780123914217.

[15] Xunren Yang. *Atmospheric Acoustics*. De Gruyter, Inc, 2016. ISBN 9780123914217.

[16] Philip M. Morse. *Vibration and Sound*. McGraw-Hill Book Company, Inc., 2nd edition, 1948. ISBN 978-0070433298.

[17] Philip M. Morse and Karl Uno Ingard. *Theoretical Acoustics*. McGraw-Hill, Inc., 1968.

[18] William M. Hartmann. *Principles of Musical Acoustics*. Springer, 2013. ISBN 978-1-4614-6785-4. doi: 10.1007/978-1-4614-6786-1.

[19] Peter Damaske, editor. *Acoustics and Hearing*. Springer-Verlag Berlin Heidelberg, 2008. ISBN 978-3-540-78227-8.

[20] J. J. Bowman, T. B. A. Senior, and P. L. E. Uslenghi, editors. *Electromagnetic and Acoustic Scattering by Simple Shapes*. North-Holland Publishing Company, 1969. ISBN 978-0720401523.

[21] R. W. B. Stephens and A. E. Bate. *Acoustics and Vibrational Physics*. Edward Arnold (Publishers) Ltd., 2nd edition, 1966. ISBN 978-0713121520.

[22] Huinam Rhee and Youngjin Park. Acoustic and Elastic Wave Scattering from A Rigid or Soft Cylinder. In *Proceedings of the Fifth International Congress on Sound and Vibration*, 1997. URL `https://www.semanticscholar.org/paper/Acoustic-Wave-Scattering-from-and-Elastic-A-Rigid-Rhee/891755f4f6c564d8eaee39b3dce205bd1a7d8221`.

[23] Miguel C. Junger and David Feit. *Sound, Structures, and Their Interaction*. The MIT Press, 1972. ISBN 0-262-10010-X.

[24] P. W. Smith Jr. Sound transmission through thin cylindrical shells. *The Journal of the Acoustical Society of America*, 29(6):721–729, 1957. doi: 10.

1121/1.1909025. URL https://www.ece.uvic.ca/~bctill/papers/numacoust/SmithJr_1957.pdf.

[25] George B. Arfken, Hans J. Weber, and Frank E. Harris. *Mathematical Methods for Physicists*. Academic Press, 7th edition, 2012. ISBN 978-0-12-384654-9. doi: 10.1016/C2009-0-30629-7.

[26] G. N. Watson. *A Treatise on the Theory of Bessel Functions*. Cambridge University Press, 1922.

[27] George L. Lamb Jr. *Introductory applications of partial differential equations with emphasis on wave propagation and diffusion*. Wiley, 1995. ISBN 978-0-471-31123-2.

[28] Eric W. Weisstein. *Hankel Function of the First Kind*. From *MathWorld*–A Wolfram Web Resource, 2021. https://mathworld.wolfram.com/HankelFunctionoftheFirstKind.html [Accessed: November 9th 2021].

[29] E. A. Skelton. Scattering of a normally incident plane wave by a rigid rectangle. In *Proceedings: Mathematical, Physical and Engineering Sciences*, volume 457, no. 2011 (Jul. 8, 2001), pages 1757–1785. Royal Society, 2001.

[30] Andreas Asheim and U. Peter Svensson. An integral equation formulation for the diffraction from convex plates and polyhedra. *Acoustical Society of America*, 133(6):3681–3691, 2013. doi: 10.1121/1.4802654. URL https://asa.scitation.org/doi/10.1121/1.4802654.

[31] Sara R. Martin, U. Peter Svensson, Jan Slechta, and Julius O. Smith. Modeling sound scattering using a combination of the edge source integral equation and the boundary element method. *Acoustical Society of America*, 144(1):131–141, 2018. doi: 10.1121/1.5044404. URL https://asa.scitation.org/doi/10.1121/1.5044404.

[32] Peter Svensson. *Edge Diffraction Matlab toolbox EDtoolbox v 0.216 Manual*, 2021. https://github.com/upsvensson/Edge-diffraction-Matlab-toolbox [Accessed: August 16th 2021].

[33] Ronald N. Miles. *Physical Approach to Engineering Acoustics*. Springer, 2020. ISBN 978-3-030-22675-6.

[34] I.V. Belyaev, A.Y. Golubev, A.Y Zverev, S. Yu. Makashov, V. V. Palchikovskiy, A. F. Sobolev, and V. V. Chernykh. Experimental investigation of sound absorption of acoustic wedges for anechoic chambers. *Acoustical Physics*, 61(5):606–614, 2015. doi: 10.1134/S1063771015050048. URL https://link.springer.com/article/10.1134/S1063771015050048.

[35] Mladen Russo, Luka Kraljević, Maja Stella, and Marjan Sikora. Acoustic performance analysis of anechoic chambers based on ISO 3745 and ISO 26101: standards comparison and performance analysis of the anechoic chamber at the University of Split. In *Proceedings of Euronoise 2018 Conference*, 2018. URL https://www.semanticscholar.org/paper/

Acoustic-performance-analysis-of-anechoic-chambers-Russo-Kraljevi%C4%87/248134c526fbdf6c221b08e06fe5241820ee3a9c.

[36] Singh K. Sushil, Mohit Garg, and S. Narayanan. Estimation of the lower cut-off frequency of an anechoic chamber: An empirical approach. *International Journal of Aeroacoustics*, 19(1-2):57–72, 2020. doi: 10.1177/1475472X20905070. URL https://journals.sagepub.com/doi/10.1177/1475472X20905070.

[37] Xiang Duanqi, Wang Zheng, and Chen Jinjing. Acoustic design of an anechoic chamber. *Applied Acoustics*, 29(2):139–149, 1990. doi: 10.1016/0003-682X(90)90027-R. URL https://www.sciencedirect.com/science/article/pii/0003682X9090027R.

[38] Isabel Expósito, Manuel García Sánchez, and Iñigo Cuiñas. Uncertainty assessment of a small rectangular anechoic chamber: From design to operation. *IEEE Transactions on Antennas and Propagation*, 68(6):4871–4880, 2020. doi: 10.1109/TAP.2020.2969842. URL https://ieeexplore.ieee.org/document/8979259.

[39] F. Alton Everest and Ken C. Pohlmann. *Master Handbook of Acoustics*. McGraw-Hill, 5th edition, 2009. ISBN 978-0-07-160332-4.

[40] AFMG Technologies GmbH, Berlin. *EASERA Users Manual v 1.2*, 2021. https://www.afmg.eu/en/easera-12-manual [Accessed: September 29th 2021].

[41] Maryam Odabaee, Mostafa Odabaee, Matthew Pelekanos, Gerhard Leinenga, and Jürgen Götz. Modeling ultrasound propagation through material of increasing geometrical complexity. *Ultrasonics*, 90(2018):52–62, 2018. doi: 10.1016/j.ultras.2018.05.014. URL https://www.sciencedirect.com/science/article/pii/S0041624X17307850.

[42] A. Bruce Carlson and Paul B. Crilly. *Communication Systems: An Introduction to Signals and Noise in Electrical Communication*. McGraw-Hill, Inc., 5th edition, 2010. ISBN 978-0-07-338040-7.

[43] Angelo Farina. Advancements in impulse response measurements by sine sweeps. In *Convention paper, presented at the 122nd Audio Engineering Society Convention, Vienna, Austria*, 2007.

[44] Adil Alpkocak and Malik Kemal Sis. Computing impulse response of room acoustics using the ray-tracing method in time domain. *Archives of Acoustics*, 35(4):505–519, 2010. doi: 10.2478/v10168-010-0039-8. URL https://www.researchgate.net/publication/271383273_Computing_Impulse_Response_of_Room_Acoustics_Using_the_Ray-Tracing_Method_in_Time_Domain.

[45] Sunil Bharitkar and Chris Kyriakakis. *Immersive Audio Signal Processing*. Springer Science+Business Media LLC, 2006. ISBN 978-0-387-28453-8.

[46] Douglas A. Abraham. *Underwater Acoustic Signal Processing*. Springer Nature Switzerland AG, 2019. ISBN 978-3-319-92981-1. doi: 10.1007/978-3-319-92983-5.

[47] Ken'iti Kido. *Digital Fourier Analysis: Fundamentals*. Springer Science+Business Media, 2015. ISBN 978-1-4614-9259-7. doi: 10.1007/978-1-4614-9260-3.

[48] Wojbor A. Woyczynski. *A First Course in Statistics for Signal Analysis*. Birkhäuser, 2006. ISBN 978-0-8176-4398-0.

[49] Jerry H. Ginsberg. *Acoustics-A Textbook for Engineer and Physicists, Volume I: Fundamentals*. Springer International Publishing AG, 5th edition, 2018. ISBN 978-3-319-56843-0. doi: 10.1007/978-3-319-56844-7.

[50] Swen Müller. Measuring transfer-functions and impulse responses. In D. Havelock, S. Kuwano, and M. Vorländer, editors, *Handbook of Signal Processing in Acoustics*, pages 65–85. Springer, 2008. ISBN 978-0-387-77698-9. doi: 10.1007/987-0-387-30441-0_5.

[51] A. Bruce Carlson and Paul B. Crilly. *COMMUNICATION SYSTEMS An Introduction to Signals and Noise in Electrical Communication*. McGraw-Hill, 5th edition, 2010. ISBN 978–0–07–338040–7.

[52] Xiang Wan, Wenqian Wang, Tiejun Tong, and Jiming Liu. Estimating the sample mean and standard deviation from the sample size, median, range and/or interquartile range. *BMC Medical Research Methodology*, 14(135), 2014. doi: 10.1186/1471-2288-14-135. URL `https://link.springer.com/article/10.1186/1471-2288-14-135`.

[53] Knud Rasmussen. *Calculation methods for the physical properties of air used in the calibration of microphones*, 1997. `https://orbit.dtu.dk/en/publications/calculation-methods-for-the-physical-properties-of-air-used-in-th` [Accessed: May 18th 2021].

[54] Peter M. Juhl and Vicente Cutanda Henriquez. *OpenBEM*, 2015. `http://www.openbem.dk` [Accessed: December 11th 2021].

[55] Ernest O. Doebelin. *Measurement Systems: Application and Design*. McGraw-Hill, Inc., 4th edition, 1990. ISBN 0-07-017338-9.

[56] Sebastian T. Prepelita, Javier Gómez Bolaños, Michele Geronazzo, Ravish Mehra, and Lauri Savioja. Pinna-related transfer functions and lossless wave equation using finite-difference methods: Validation with measurements. *The Journal of the Acoustical Society of America*, 147(3631), 2020. doi: 10.1121/10.0001230. URL `https://asa.scitation.org/doi/10.1121/10.0001230`.

[57] Brüel & Kjær A/S. *Technical Documentation, Microphone Handbook, Vol. 1: Theory*, 2019. `https://www.bksv.com/doc/be1447.pdf` [Page 3-10. Accessed: December 13th 2021].

[58] Isabel Berg. *"master-thesis" at Github, collection of scripts used for master thesis*, 2021. `https://github.com/IB-IsabelBerg/master-thesis` [Accessed: December 11th 2021].

[59] Brüel & Kjær A/S. *Product Data: TEDS microphones*, 2016. https://www.bksv.com/en/transducers/acoustic/microphones/microphone-set/4190-l-001 [Accessed: December 4th 2021].

[60] SEAS of Norway. *Product Data: Tweeter 25TFFN/G*, 1996. http://www.seas.no/images/stories/vintage/pdfdataheet/h0615_25tffng.pdf [Accessed: December 4th 2021].

[61] Aurasound. *Product Data: NSW1-205-8A*, 2003. https://www.madisoundspeakerstore.com/approx-1-fullrange/aurasound-nsw1-205-8a-1-extended-range/ [Accessed: December 4th 2021].